Sugars, the main energy source for the human metabolism and an integral part of many biological systems, is also a core dietary element within the modern human diet. New processing forms of these materials (e.g. electrospun sugar nanofibers), had led to new applications beyond nutrition, like cosmeceuticals, healthcare and others. Electrospinning is a widely-known method for producing nanofibers from a wide range of materials. In this work, the electrospinnability mechanisms of concentrated saccharide solutions, cyclodextrins, modified sucrose compounds and food grade glucose syrup is discussed. Furthermore, the relationship between the rheological behavior of the solutions, current electrospinnability models and the significance of intermolecular forces in the electrospinnability of these materials is also widely discussed. New experimental evidence on the electrospinnability of saccharides related to their physical-chemical properties, is provided. Furthermore, the commercial application of the research on the electrospinnability of saccharide materials, is exemplified with the development of mānuka honey- glucose syrup nanofibre composite membranes.

Dr. Pablo Gerardo Torres Lepe received his Ph.D. in Mechanical Engineering from the Univ. of Canterbury, New Zealand and Bachelor of Sciences in Chemical Engineering from the Univ. of Guadalajara, México. An bio-nano-agritech entrepreneur and a passionate scientist, with extensive networks across a wide range of industries all around the world.

978-3-659-77250-4

Pablo Lepe

Nano-candyfloss

LAP LAMBERT Academic Publishing

Pablo Lepe

Nano-candyfloss

Pablo Lepe

Nano-candyfloss

LAP LAMBERT Academic Publishing

Imprint
Any brand names and product names mentioned in this book are subject to trademark, brand or patent protection and are trademarks or registered trademarks of their respective holders. The use of brand names, product names, common names, trade names, product descriptions etc. even without a particular marking in this work is in no way to be construed to mean that such names may be regarded as unrestricted in respect of trademark and brand protection legislation and could thus be used by anyone.

Cover image: www.ingimage.com

Publisher:
LAP LAMBERT Academic Publishing
is a trademark of
International Book Market Service Ltd., member of OmniScriptum Publishing Group
17 Meldrum Street, Beau Bassin 71504, Mauritius

Printed at: see last page
ISBN: 978-3-659-77250-4

Nano-candyfloss

Dr. Pablo G. T. Lepe [1,2*]

[1] *Revolution Fibres Ltd., 9a Corban Ave., Henderson 0612, Auckland, New Zealand.*

[2] *Department of Mechanical Engineering, University of Canterbury, Private Bag 4800, Christchurch 8140, New Zealand.*

**Corresponding author: Pablo Lepe, Tel: +64 21 1469938, E-mail: pablo@innovanano.org*

Abstract: Sugars, the main energy source for the human metabolism and an integral part of many biological systems, is also a core dietary element within the modern human diet. New processing forms of these materials (e.g. electrospun sugar nanofibers), had led to new applications beyond nutrition, like cosmeceuticals, healthcare and others. Electrospinning is a widely-known method for producing nanofibers from a wide range of materials. In this chapter, the electrospinnability mechanisms of concentrated saccharide solutions, cyclodextrins, modified sucrose compounds and food grade glucose syrup is discussed. Furthermore, the relationship between the rheological behavior of the solutions, current electrospinnability models and the significance of intermolecular forces in the electrospinnability of these materials is also widely discussed. New experimental evidence on the electrospinnability of saccharides related to their physical-chemical properties, is provided. Furthermore, the commercial application of the research on the electrospinnability of saccharide materials, is exemplified with the development of mānuka honey-glucose syrup nanofibre composite membranes.

Keywords: Sugar, nanofiber, saccharide, electrospinning, hydrogen bonding, Van der Waals forces.

1.1 INTRODUCTION

Carbohydrates having at least one glucose molecule ($C_6H_{12}O_6$) within their structure, are commonly referred to as saccharides and usually divided into four categories: monosaccharides, disaccharides, oligosaccharides, and polysaccharides. Saccharide-based materials are the energy storage medium for many living organisms and the most basic structural component of many biomaterials [1]. Oligosaccharides are carbohydrates that consist of monosaccharide units linked together by short chains of varying length (di-, tri-, tetra-, pentasaccharides, etc.) [2]. Each monosaccharide unit (6 carbons) may exist in either the pyranose (6-ring) or furanose (5-ring) form [3]. For example, raffinose ($C_{18}H_{32}O_{16}$), composed of glucose, fructose and galactose is the most common naturally occurring trisaccharide.

Fructose is an isomer of glucose, both have the same molecular formula ($C_6H_{12}O_6$) but differ structurally. Fructose has a more stable furanose structure (five carbon ring), called ketose. Glucose has a more flexible pyranose (six carbon ring) configuration, called aldose. Glucose (D-glucopyranose) in aqueous solution exists mostly in its cyclic pyranose form, as it readily undergoes isomerism [2]. In contrast, fructose (D-fructo-furanose), being the most stable isomer, does not dissociate (donate a proton) as easily as glucose. In other words, isomerism is caused by the chirality (D-, L-) of the anomeric carbon (C-1) per monosaccharide resulting in two different stereoisomers (trans α-, cis β-) which can in turn exists in either pyranose (6-ring) or furanose (5-ring) form [4]. Both glucose and fructose are reducing sugars because of the capacity to convert to their open-chain form through isomerization (e.g., aldehyde group in glucose) or tautomerization (e.g, ketone group in fructose) of its structure their (glucose) and (fructose), as these group readily undergo mutarotation [3]. Such physical-chemical property is particularly relevant during thermal processing, such as sugar caramelization. Mutarotation can momentarily produce dihexose sugars and other metastable and more intricate carbohydrate chain structures [5]. In contrast, disaccharides like sucrose ($C_{12}H_{22}O_{11}$), have glycosidic bonds between the glucose (C-1) and fructose (C-4) anomeric carbons and thus cannot convert to an open-chain form [6]. However, maltose ($C_{12}H_{22}O_{11}$), typically produced during glucose caramelisation (e.g., sugar syrups) and an isomer of sucrose, is a reducing sugar as they are linked by a (C_1-C_4) glycosidic bond [2].

Candyfloss is a thermal-mechanical process of extrusion where pressurized air and concentrated sugar solutions, are supply through small holes within a centrifuge. Melt-spun sugar fibers are then collected into a rod or plate, mostly containing air within their foamed matrix structure. In general, the spinnability of a filament is controlled by the relaxation time and tensile strength of the material, according to the theory of cohesive fracture [7]. Instability due to cohesive fracture commonly occurs in melt-spinning of high molecular weight materials due to their relatively long relaxation time (1 s). Cohesive fracture is a form of viscoelastic instability, for which the loss modulus is higher than the storage modulus. In general, longer relaxation times, higher stretching velocities and larger draw ratios will tend to encourage cohesive fracture [7, 8]. However, there are many other types of flow instabilities that affect filament formation, such as hydrodynamic instabilities [9-11]. For example, Ziabicki showed that the capillary flow instabilities were the determining factor in the spinnability of solutions having low viscosity and low jet velocity. In contrast, elasticity appears to be the limiting condition for spinnability at higher viscosities and velocities [7].

Electrospinning is a method of producing fibres in the micro and nano dimensional scale, this is between 1 x 10^ (-9)m (1 nm) and 1 x 10^(-7)m (0. 1 µm). During the electrospinning process, a high voltage is applied to a droplet of a polymer solution (or melt), stretching the droplet into a conical shape (known as the Taylor cone) by means of electrostatic repulsion. A jet of polymer solution is emitted from the tip of the Taylor cone if the build-up of internal electrical charge overcomes the surface tension of the droplet. Given an appropriate combination of electro-viscoelastic properties, the polymer jet initially follows a stable, linear trajectory that resists the Plateau-Rayleigh instability, enabling it to be drawn into a fiber. Otherwise, the solution will break-up into small droplets during flight, as described by the Rayleigh instability (aka electrospraying). The whipping instability is a very rapid phenomenon, with axial strain rates of about 105 s-1 [12]. At this strain rate, the whipping instability leads to further reduction of the jet thickness from around 100 µm down to 100 nm, in less than a fraction of a second [13] (Figure 1).

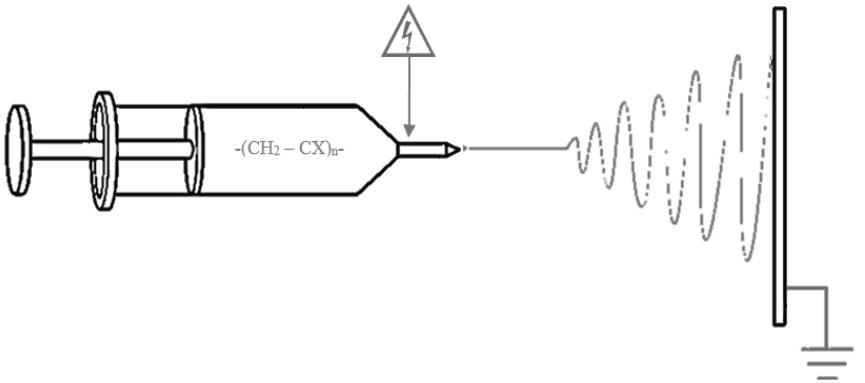

Figure 1. Electrospinning process diagram.

The ability of a polymer solution to resist the Plateau-Rayleigh instability during flight is usually attributed to the entanglement of polymeric molecules, and chain entanglement is commonly proposed to be the leading mechanism of fiber formation during electrospinning of polymeric systems. The formation of uniform electrospun polymeric fibres is thought to rely on the presence of at least 2 to 2.4 entanglements per chain, based on the critical theta concentration or pervaded volume threshold of each polymer-solvent system. However, some polymers may transition from electrospraying to electrospinning (as evidenced by the formation of beads-on-a-string) at concentrations between the critical overlap concentration ($c*$) (i.e. semi-dilute, un-entangled) and the entanglement concentration (Ce) (i.e. semi-dilute, entangled), where Ce is typically ~$10 \times c*$. The critical overlap concentration for entanglement $c*$ corresponds to the maximum number of polymer chains with a radius of gyration r that can be fitted inside the volume of a sphere ($v= 4/3*\pi*r3$) where steric exclusion due to increased excluded volume effects starts to overlap the chains [68, 111, 155].

An alternative approach used to describe the concept of electrospinnability is the visco-elasto-capillary theory. According to visco-elasto-capillary thinning theory, non-Newtonian fluids that undergo shear thinning and where $G' > G''$ at higher angular frequencies are able to better resist extensional capillary thinning and filament break-up when compared with Newtonian fluids for which $G' < G''$ at lower angular frequencies. According to the visco-elasto-capillary theory, when the

inverse of the fluid's relaxation time exceeds the rate of capillary thinning (wave propagation), Rayleigh instabilities can be suppressed; resulting in uniform fibres [15, 16]. Moreover, elasticity for supramolecular materials is often related to electrospinnability, through gelation or colloid aggregation via a hydrogen bonding network and Van der Waals mechanisms. For example, computational models for low viscosity and dilute polymer solutions, have shown that relaxation times of polymer chains due to an extensional change in filament radius far exceed the estimated values using conventional Rouse–Zimm theory [14, 116]. Typically, relaxation times for polymers are in the range of 1 to 3 seconds [15]. However, relaxation processes that occur on smaller time scales than 10–100 ms cannot be unambiguously resolved [16]. The visco-elasto-capillary theory sets different boundaries for electrospinnability that depend on the rheological properties of the solution (Figure 2). This can be generally described by the intrinsic Deborah number (De)

$$〖De〗_{intrinsic}=\lambda/〖[\rho*(L/\text{ɤ})]〗^{(1/3)} \qquad \text{equation 1}$$

where $De_{intrinsic}$ equals the relaxation time λ divided by the cubic root of the density ρ, multiplied by the factor of the length scale L divided by the surface tension ɤ; and by the Ohnesorge number (Oh)

$$Oh=Ca/Re=(((\eta*v)/\text{ɤ})/(((v*L*\rho)/\eta) \qquad \text{equation 2}$$

where the capillary number Ca equals the zero-shear viscosity η multiplied by the jet speed v and in total, divided by the surface tension ɤ. According to the visco-elasto-capillary theory, a solution can be considered electrospinnable, if the rheological properties comply with the following condition De (elasticity) ≥ Oh (viscosity) ≥ 1 [16]. In other words, a build-up of electrical stresses in the jet will suppress Rayleigh instabilities if the extensional deformation rate caused by the electrical stresses is faster than the inverse of the relaxation time of the fluid, resulting in uniform filaments [17]. In turn, the elasto-capillary thinning rate of the filament should scale with λ-1, where λ is the characteristic material relaxation time (Figure 2). Subsequently, the growth rate of the filament disturbances, should also scale with the inverse of the Rayleigh time scale for inertia capillary break-up.

$$"\lambda=" \ 1/\sqrt{((\rho L^3)/\text{ɤ})} \qquad \text{equation 3}$$

where ρ is the density of the fluid, L3 is the volume of the capillary and ɤ the surface tension between the fluid and air. Hence, λ-1 requires the intrinsic Deborah number to be greater than 1 [15,17,18]. In contrast, for Deborah numbers below unity, elastic effects do not stabilise the jet and Newtonian-like break-up dynamics are observed.

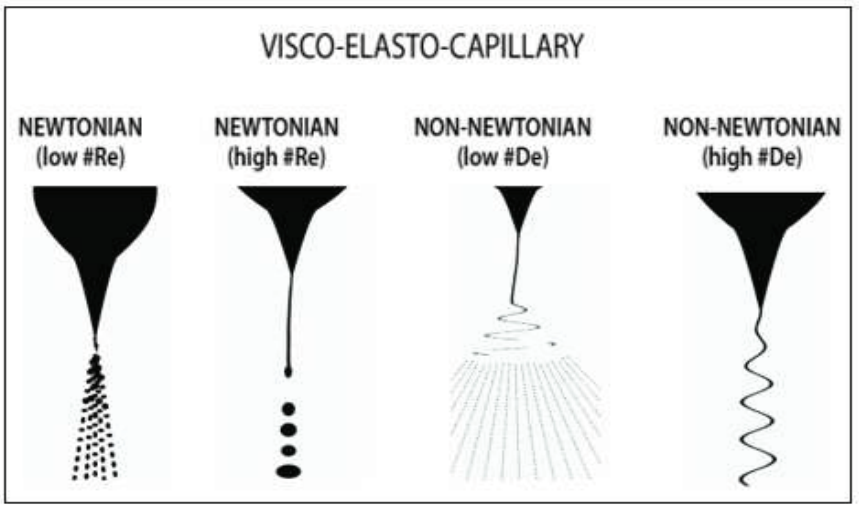

Figure 2. Representation of the visco-elasto-capillary theory and its correlation to jet formation, showing the transition from intermittent spraying (low # Re) to stable spinning (high #De). Re is the Reynolds number ($Re = (\rho Lv)/\eta$) and De is the intrinsic Deborah number ($De = (\lambda \text{ material})/(\text{Rayleight time scale})$) [15].

However, visco-elasto-capillary theory, similar to chain entanglement theory, is also based on non-Gaussian conformational statistics for relatively long macromolecules, as well as on the physical-chemical scaling concepts of de Gennes commonly used in polymer physics [19, 20]. In other words, neither theory considers reversible bonding (sticky reptation) by hydrogen bonding nor van der Waals forces, as a critical parameter for the unusual relaxation times of the saccharide electrospinning. For instance, electron-dynamic interactions such as Lifshitz–van der Waals interactions can promote an asymmetric electronic configuration of the molecules within the solution when aqueous solutions of nonpolar molecules are subjected to high voltage electric

fields [10, 11]. Moreover, Lifshitz–van der Waals interactions can arise from permanent dipole-dipole interactions (Keesom interactions), dipole-induced dipole (dispersion) interactions (London forces), and dipole-induced dipole (induction) interactions (Debye polarisation). In addition, the orientation of charged water molecules is in turn associated with the high density of opposing electron-donors, often a sizeable distance away from the hydrophobic (electron-donating) surfaces – a mechanism associated with hydrogen bonding [10, 11]. Furthermore, reported evidence on the electrospinnability of nonpolymeric systems suggests that their capacity to be electrospun is dependent on complex secondary chemical bonding and on the electro-viscoelastic interactions between individual molecules [21-30]. For example, polysaccharide electrospinnability has been reported to be particularly dependent on hydrogen bonding [27, 31, 32]. Also, the presence of hydrogen bonding mechanisms is thought to influence the electrospinnability of food-grade polysaccharide solutions [33, 34]. Likewise, hydrogen bonding between α-, β- and γ- cyclodextrin (CD) molecules and hydrocolloids are thought to be responsible for the electrospinnability of highly concentrated aqueous solutions of CDs [24-27, 31, 35-38].

The significance of intermolecular forces in the electrospinnability of modified sucrose compounds (i.e. Octa-O-acetyl sucrose and Octa-O-methyl sucrose) has been investigated as a function of the substitution of sucrose, using an aqueous sucrose solution as the control. The significance of non-covalent interactions in the electrospinnability of 2-hydroxypropyl-β-cyclodextrin (2HP-β-CD) was further investigated, as hydrogen bonding has been reported to play a role in promoting the electrospinnability of cyclodextrins. The rheological behavior of 2HP-β-CD solutions was characterized by a frequency-independent stress relaxation plateau such as that observed in cross-linked polymer networks and reversible polymer gels with non-linear viscoelasticity. The results presented throughout this chapter indicate that saccharide electrospinnability does not depend on physical entanglements, as described by the chain entanglement model. Instead, the electrospinnability of concentrated saccharide solutions is in agreement with visco-elasto-capillary theory, as described by the Deborah (De) and Onsager (Oh) non-dimensional numbers relating elastocapillary thinning rates to the characteristic material's relaxation times.

However, determining the electrospinnability of a given material is a complex problem that involves the consideration of many different solution and process parameters. Common theories based on polymer physics and rheology cannot accurately describe the electrospinning behaviour of nonpolymeric systems, such as supramolecular systems with extensive secondary bonding (e.g., saccharide solutions).

1.2 SUGAR BASED BIOMATERIALS AND THEIR ELECTROSPINNABILITY

Oligosaccharide and polysaccharide materials are well known for their ability to form fibres by electrospinning [3, 33, 34, 40, 41]. The electrospinning of biopolymers and their applications is widely reported in the literature [22, 37, 39]. However, there is no previous report on the electrospinnability of sugars. Honey, a highly-valued food commodity with many prebiotic, antimicrobial and health benefits, is usually composed of 38% fructose, 30% glucose, 1% sucrose/maltose, 9% other sugars, and 22% water, with; containing varying amounts of several suspended solids (oils, flavonoids, polyphenols, etc.) [42]. Honey from native New Zealand mānuka plants (Leptospermum scoparium) is a high valued commodity in many parts of the world, especially in Asia (> $1.0 NZD/g). Antimicrobial effects against a wide range of gram-positive and gram-negative bacteria are well-known properties of mānuka honey.

The electrospinning of complex oligosaccharides and cyclic polysaccharide materials such as cyclodextrins have also been broadly reported [24-26, 31, 35-37]. Likewise, the electrospinnability of emulsions, sol-gel systems and complex supramolecular materials have been also reported in the literature [41, 43-49]. Cyclodextrins are able to host a wide range of small hydrophobic molecules (or inclusions) within their hydrophobic interior cavity. In contrast, the exterior of the cyclodextrin molecule is highly hydrophilic, providing the inclusion- cyclodextrin complexes with water solubility (Figure 3) [50].

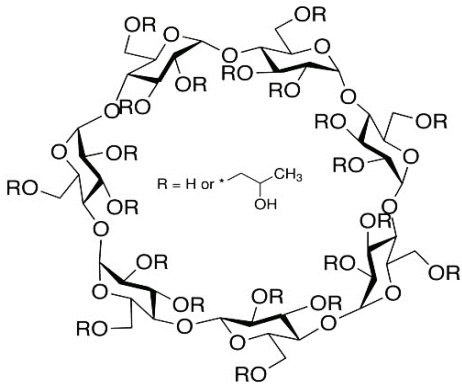

Figure 3. Chemical structure of tested 2-hydroxypropyl-β-cyclodextrin (2HP-β-CD), with a molecular substitution per anhydrous glucose unit between 0.57 and 1.29 $(C_6H_9O_5)_7(C_3H_7O)_{4.5}$

CDs are often used as carriers for solubilising hormones, vitamins, drugs, and other compounds frequently used in tissue and cell culture and pharmaceutical applications [25, 26, 37, 51]. For example, the complexation of mānuka honey with *a*-cyclodextrin has been reported to have prebiotic effects during digestion, due to the increased antimicrobial activity of the mānuka honey CDs complexes [52].

Interestingly, amorphous structure on the cyclodextrin nanofibers was shown across all samples as confirmed by atomic force microscopy (AFM), X-ray powder diffraction (XRD), thermogravimetric analysis (TGA) and differential scanning calorimetry (DSC) [27]. Also, Manasco et al., observed that the electrospinnability of HP-*β*-CD is reduced in the presence of urea salts [53]. Urea is known to be a chaotropic agent, disrupting hydrogen bonding between water molecules [54]. Urea can also affect the hydrogen bonding between CD molecules and bound water, reducing the size of the CD aggregates [55]. Similarly, Celebiouglu et al., considered the influence of hydrogen bonding on the electrospinnability of aqueous HP-*β*-CD solutions by adding urea salts to hinder electrospinnability [38]. Nonetheless, discussions regarding the hydrogen bonding maker or breaker capacity of urea for disrupting the tetrahedral configuration of the water stereochemistry, are still not resolved [54, 56]. Argumentation is centered on the capacity of urea to slow down the rotational dynamic of water, by geometrically altering hydrogen bonding networks and water stereochemistry [56].

Also, it has been reported that the hydrogen bonding capacity of aqueous HP-β-CD solutions is affected (as increased CD solubility) by using heavy water as a solvent and by the addition of sodium salts, among others additives [55]. Likewise, ethanol-water mixtures have shown to strengthen the hydrogen bonding between respective solvent molecules [57]. Moreover, polar solvents, such as acetone, can also have hydrogen bonding structuring effects on water [58]. Likewise, conductivity, surface tension and pH of aqueous CDs solutions can affect CD-water aggregate formation and consequent electrospinnability [54, 55-58].

Moreover, the influence of pH and noncovalent intermolecular bonding on electrospinnability is also acknowledged in polymeric systems [28-30, 59]. For instance, pH and hydrogen bonding are known to influence the electrospinnability of polymethyl methacrylate and polyvinyl alcohol [29, 30]. For such polymeric systems, rheological studies have shown that pH and hydrogen bonding directly affect the viscoelastic properties of aqueous and nonpolar solutions. For example, the viscoelasticity of aqueous HP-β-CD solutions appears to be dependent on the strength of the hydrogen bonding between CD molecules [53]. Therefore, aqueous HP-β-CD solutions exhibit solid-like behaviour, as indicated by a storage modulus (G′) that exceeds the loss modulus (G″) [53]. Moreover, the formation of molecular aggregates of aqueous CDs can be attributable to depletion flocculation by extensive hydrogen bonding networks [25-27]. However, the effect of van der Waals forces in the electrospinnability of such materials is not acknowledged. Similarly, the potential of saccharides to create metastable supramolecular-like architectures may underpin their molecular aggregation [4].

The electrospinning of food related proteins such as collagen [21, 60-62], zein [63-68, 71], bovine serum albumin [69], gelatin [72, 73] and others [70, 74] are often focused on medical and cosmeceutical applications [61, 75, 76]. The electrospinning of biopolymers such as chitosan [21, 77-82] and cellulose-based materials [83-86] has been widely reported in literature for various applications [77-86]. Low molecular weight saccharides have applications in medicine, biology and microbiology [87] as well as in electrochemistry and nanotechnology [4].

Commercial applications of biopolymer-based materials for smart nanofibre composite membranes are rapidly growing, especially for tissue engineering, medical wound dressings, and cosmetic patches [39, 73-76,

88-91]. Also, polysaccharide applications have commercial significance [33, 34], both as dynamic materials for complexation [92, 60] and as functional carriers for bio-active compounds [88]. A particularly significant effect of using biomaterials in aqueous systems during electrospinning, is the possibility of reducing the environmental and human health impact of toxic solvent systems in commercial nanofibre manufacturing [46]. Additionally, the possibility to create nanofibre membranes by emulsion electrospinning is particularly significant to the growing nanofibre manufacturing industry [43, 45, 93, 94], as emulsion systems could require less regulatory constrains during production. Also, the relative ease for the complexation of drugs in emulsions and colloidal systems facilitates the commercialization of new delivery technologies to the medical and pharmaceutical markets [95-99].

Pharmaceutical, cosmeceutical and biotechnology applications for polysaccharide materials are often successfully commercialized in the food, pharmaceutical and cosmeceutical industries [4, 33, 34, 39, 41]. For example, polysaccharide electrospun nanofibre (e.g., alginates, cellulose, chitin, chitosan, hyaluronic acid, starch, dextran, heparin and levan) could be used for enzyme immobilization for biotechnology processes or as new drug delivery mechanisms for wound dressings [33, 34, 41]. Also, the electrospinning of new saccharide solutions could potentially lead to the development of new devices for bio-sensing, skin scaffolds, and personal health products [75].

1.3 NEW EXPERIMENTAL EVIDENCE ON SACCHARIDE ELECTROSPINABILITY – NANOCANDYFLOSS

The electrospinnability of concentrated aqueous solutions of glucose, fructose and sucrose was combinatorially studied by physicochemical and rheological characterisation methods, and by subsequently examining the fiber morphology via scanning electron microscopy. Furthermore, the significance of intermolecular forces (van der Waals versus hydrogen bonding) in the electrospinnability of saccharides was investigated as a function of the substitution of sucrose (e.g., octa-*O*-acetyl sucrose and octa-*O*-methyl sucrose), using an aqueous sucrose solution as the control. Additionally, the electrospinnability of cyclodextrin solutions was also

studied in order to explore the effects of hydrogen bonding on supramolecular materials with complex visco-elasticity. Therefore, the electrospinnability of 2-hydroxypropyl-β-cyclodextrins (2HP-β-CD) was investigated by comparing a 2HP-β-CD peroxide-aqueous/acetone-ethanol/NaHCO3 solution and an aqueous urea solution, as a function of 2HP-β-CD concentration. Also, the electrospinnability of food-grade glucose syrup was investigated in order to explore affordable manuka honey nanofibre formulations for commercial applications.

1.3.1 Methodology

1.3.1.1 *Materials*

D-glucose ($C_6H_{12}O_6$ > 99.5%, CAS # 50-99-7) D-sucrose ($C_{12}H_{22}O_{11}$ > 99.5%, CAS # 57-50-1), D-fructose ($C_6H_{12}O_6$ > 99%, CAS # 57-48-7), Raffinose ($C_{18}H_{32}O_{16} \cdot 5H_2O$ > 99%, CAS # 17629-30-0), and maltose ($C_{12}H_{22}O_{11} \cdot H_2O$ > 99%, CAS # 6363-53-7) were used as supplied (Sigma-Aldrich, Germany) without further purification. Urea (CH_4N_2O > 99.5%, CAS # 57-13-6), sodium hydrogen carbonate ($NaHCO_3$ > 99.7%, CAS # 144-55-8) and aqueous hydrogen peroxide (H_2O_2 > 50 wt. %, CAS # 7722-84-1) were also used as supplied (Sigma-Aldrich, Germany) without further modification (Table 1). Seebio Biotech, Inc, Shanghai, China supplied the 2-hydroxypropyl-β-cyclodextrin (2HP-β-CD) powder ($(C_6H_9O_5)_7 \cdot (C_3H_7O)_{4.5}$) with an averaged degree of substitution of 4.5 (CAS # 128446-35-5; molar mass 1541.5 g/mol and molecular substitution per anhydrous glucose unit between 0.57 and 1.29). Octa-*O*-acetyl sucrose ($C_{28}H_{38}O_{19}$, CAS # 116015-75-6) and Octa-*O*-methyl sucrose ($C_{15}H_{26}O_{12}$, CAS # 126-14-7) were manufactured at the organic synthesis laboratory in the Chemistry Department of the University of Canterbury, Christchurch, New Zealand.

1.3.1.2 *Solution preparation*

All tested materials were diluted in deionised water (10 µS/cm, pH 6.9) prepared using the following procedure: a) Slow solvent aggregation to a previously known amount of solute, b) Gradual heating of the aqueous solutions on a water bath until full solvation was achieved (50˚C to 75˚C) and c) Subsequent storage of the concentrated solutions into plastic tight

sealed containers. The supersaturated solutions were prepared by increasing the dissolution temperature to 75 ± 2°C for short periods of time, and then promptly storing the solutions at lower temperatures (50°C ± 2°C) in air-tight sealed containers to avoid precipitation. All solutions were prepared, processed and characterised in triplicate. All sealed solution containers were stored inside the Marford photoelastic stress freeze cabinet at 50°C ± 2°C. Subsequently, all of the physical properties of the solutions were measured at 50°C ± 2°C to avoid further precipitation of the saccharides. Density was measured on a Mettler-Toledo (XPE) analytical microbalance. All solution processing was carried out at 50°C ± 2°C to minimise the thermal variability of the materials physical-chemical properties.

1.3.1.3 *Electrospinning*

For the laboratory scale production, a modified Electrospinz ES1™ machine was used throughout the experimentation. Instead of the gravity-assisted flow system, a syringe pump (NE-500, New Era Pump Systems Inc., NY, USA) was used to deliver the electrospinning solution to the spinneret (metal hypodermic syringe needle, internal diameter of 0.3 mm) at a flow rate of 0.3 µl/min. All solutions were supplied to the spinneret at a temperature of 50°C ± 2°C, using a custom-built heating coil jacket for the glass syringe, since the solutions were considerably too viscous to be delivered to the spinneret at room temperature (20°C). The modified electrospinning apparatus ES1™ was enclosed in a grounded Faraday cage at a temperature and relative humidity of 35°C ± 1°C and 38 ± 3 %, respectively. Electrospinning of the various solutions was performed using an applied voltage of +15 kV and a spinneret-to-collector distance of 15 cm, resulting in an electric field strength (E) of 1 ± 0.02 kV/cm. A Glassman high voltage power supply (EQ series with reversible polarity) was used instead of the provided EMCO power supply of the ES1™ machine. The polarity of the applied voltage was not found to influence the electrospinnability of any of the tested solutions, indicating that the test solutions have a polarity-independent charge-carrying capability. Electrospun specimens were collected using a grounded aluminum foil substrate and subsequently stored in a temperature-controlled desiccator at low ambient humidity prior to characterisation by microscopy. For the industrial scale production of some of the materials, the Komodo™ "sonic" electrospinning system, at the Revolution Fibres production site

in Auckland, was used for prototype and product development.

1.3.2 Characterisation methods

1.3.2.1 *Physical-chemical properties of the solutions*

The average values of pH, electrical conductivity and surface tension of the solutions were measured in triplicate at a temperature of 50°C ± 2°C. The pH of the solutions was measured using a pH meter (Seven Easy, Mettler-Toledo GmbH, Greifensee, Switzerland), with a claimed precision of ± 0.02. The surface tension was measured using an optical goniometer (KSV CAM200, KSV Instruments Ltd., Finland). The electrical conductivity of the solutions was measured using a conductivity meter (EDT Instruments, RE387TX, Dover, United Kingdom), with a claimed precision of ± 0.5 %.

1.3.2.2 *Process imaging*

A high-speed motion camera (MotionPro® X3) with sensitivity of 1280 × 1024 pixels was used for capturing photographic images of the jet during flight. The fibre in flight was illuminated by six 12 V/50 W halogen lamps to provide consistent lighting conditions during video capture.

1.3.2.3 *Rheometry*

The rheological behaviour of tested materials was measured using an Anton Paar MCR series rheometer (Anton Paar GmbH, Graz, Austria). All experiments were performed at a temperature of 50°C ± 1°C with a cone and plate configuration having a 50 mm diameter and 2° angle between the surface of the cone and plate. Unavoidable least pre-shear calibration forces were automatically exerted by default settings on tested solutions, immediately after the highly viscous solutions were deposited on the rheometer plate, prior to testing. The rheological properties were measured in rotational mode as a function of the shear rate (0.1–1000 s^{-1}), and in oscillatory mode with a strain of 0.1 % as function of the angular frequency (0.1–1000 s^{-1}). A strain of 0.1 % was determined to be within the linear viscoelastic range of the solutions as determined from a strain

sweep. Zero-shear viscosities were given by fitting the complex viscosity data from the oscillatory tests using the Cox/Merz relation at an averaged viscosity of $0.1s^{-1}$. Both storage and loss moduli were measured in angular (oscillatory) mode. The zero-shear viscosity was determined from the complex viscosity data obtained by oscillatory tests using the standard Cox–Merz relation at an average shear rate of 0.1 s-1. The storage (G′) and loss (G″) moduli were measured in oscillatory mode over an angular frequency (ω) range of 0.1-1000 s-1.

1.3.2.4 *Scanning electron microscopy*

The microstructures of the electrospun samples were examined with scanning electron microscopy (SEM, JEOL JCM-5000 NeoScope Tokyo, Japan). Specimens were observed by secondary electron imaging without the use of a gold or carbon sputtered coating, at an accelerating voltage of 10 kV in high vacuum mode.

1.3.2.5 *High performance liquid chromatography (HPLC)*

Sample preparation was carried out by dissolving a weighed amount of syrup in 1 mL of reverse osmosis-purified water. After centrifugation at 14000 rpm for 10 min, the supernatant was placed in a HPLC vial. Retention times and response factors generated by calibration standards of known sugars were used to identify and calculate concentrations of the unknown components. The concentrations were compared against three different points of the calibration curves for each sugar, and the results obtained had a coefficient of determination (r^2) close to unity (0.999). HPLC analysis was carried out using a Waters 2690 Pump, auto-sampler and Econosphere 5 micron amino column at 30°C. An isocratic mobile phase of 75.0 % acetonitrile: water was used. Eluted sugars were detected using a Waters 2414 refractive index detector at 40°C.

1.3.2.6 *Non-dimensional numbers equations*

The relaxation time for each solution was approximated by the relaxation modulus based on the tube model ($\lambda = k(G')/k'(G'')$). Calculated values for each solution are not shown. Values for the relaxation times of tested solutions, using currently available rheological techniques, varied from

9s for F/+SAT solution to 0.04 s for GS/+SAT solution. Graphs of the experimental data fitting using a simplified version of the tube model, $\lambda = k(G')/k'(G'')$, are not reported.

1.3.3 Glucose, Fructose and Sucrose

The naming of the various solution compositions was abbreviated as follows: glucose (G), fructose (F), sucrose (S), glucose-fructose-sucrose (GFS), glucose-fructose (GF) and glucose-sucrose (GS). Additionally, the samples were labelled according to the concentration regime: undersaturated (-SAT), saturated (SAT) and supersaturated (+SAT). For example, FS/+SAT indicates a supersaturated solution with equal amounts of both fructose and sucrose. Electrospinnability for tested materials was evaluated based on the foremost continuous and abundant filament formation, notwithstanding droplet formation and beaded filament structure. F/+SAT and S/+SAT and solutions and their combinations exhibited the best electrospinnability results, in comparison with glucose containing solutions (Figures 4-6).

However, both G/SAT and F/+SAT solutions showed filament formation (Figure 4). Likewise, the ternary combination of glucose, sucrose and fructose /+SAT solution also showed filament formation (Figure 6). In contrast, both glucose and sucrose /SAT and /+SAT solutions did not show any filament formation. Both stable jet formation and chaotic whipping instability were observed for most sucrose-containing solutions at supersaturated concentrations (Figure 5). In particular, F/+SAT showed the longest straight jet for the pure saccharide solutions, as evidenced by their continuous filament formation.

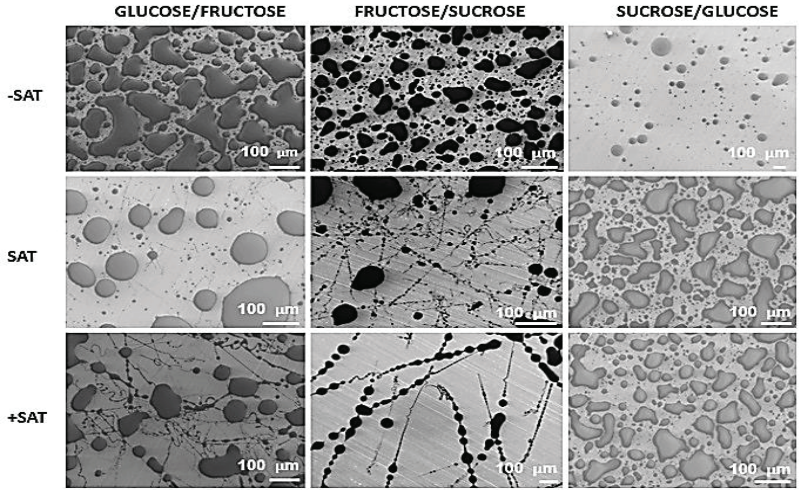

Figure 4. Scanning electron micrographs of submicron droplets and filaments of the pure saccharide solutions produced by electrospinning at 50˚C.

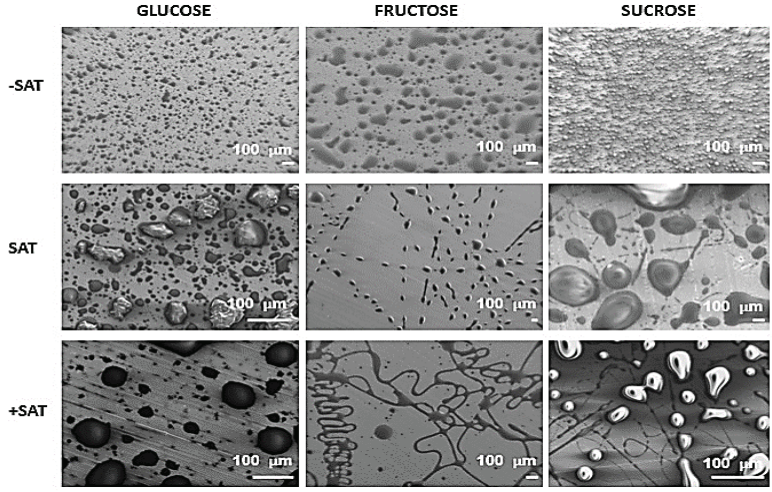

Figure 5. Scanning electron micrographs of submicron droplets and filaments of the binary saccharide solutions produced by electrospinning at 50˚C.

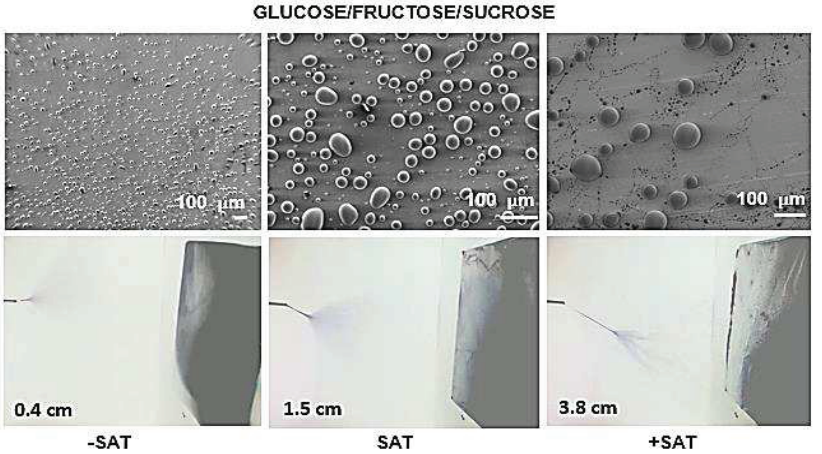

Figure 6. Scanning electron micrographs and high-speed photographs of submicron droplets, filaments and jets of the ternary saccharide solutions produced by electrospinning at 50˚C.

1.3.3.1 *Physical-chemical properties of solutions*

The highest density (1.61 g/mL), electrical conductivity (4.39×10^{-4} S/m), and surface tension (12.109 N/m) was found for FS/+SAT, GFS/-SAT, and GS/+SAT, respectively. In contrast, the lowest density (1.36 g/mL), conductivity (0.03×10^{-4} S/m), and surface tension (7.687 N/m) was found for G/-SAT, F/+SAT, and G/-SAT, respectively. Higher densities related to greater electrospinnability (Figure 7). However, lower conductivities at higher concentrations promoted filament formation (Figure 9). However, no obvious relationship between surface tension and electrospinnability was observed (Figure 8). The average standard deviations for the density, conductivity and surface tension were 0.0617 g/mL, for 0. 228 10^{-4} S/m and 0.4457 N/m, respectively. Circled areas on all graphs (Figures 7-10) exhibited the highest electrospinnability, taken as the formation of the longest continuous filaments with stable jet formation. In contrast to the expectation that relatively higher conductivities correspond to higher ionic mobility, hence increased electrospinnability, samples with lower conductivities electrospun best [193].

Moreover, electrospinnable solutions corresponded to higher pH values of tested solutions, e.g., F/+SAT (5.8) and S/+SAT (5.0), GF/+SAT (4.8)

and FS/+SAT (4.3). Although pH for tested saccharide solutions was rather acidic, this phenomenon is in agreement with other literature reporting low pH values for caramelised syrups [101]. Lower conductivity values could suggest that charge during electrospinning may not be solely transported by ionic diffusion. Likewise, an increase in jet length was observed to correlate with the formation of continuous filaments (Figure 11).

Surface tension, conductivity and viscoelasticity are important factors in the electrospinnability of any given material. However, in the case of most biopolymers and supramolecular polymers, such properties find their origin in secondary chemical forces, rather than in covalently physical bonding mechanisms [102-105].

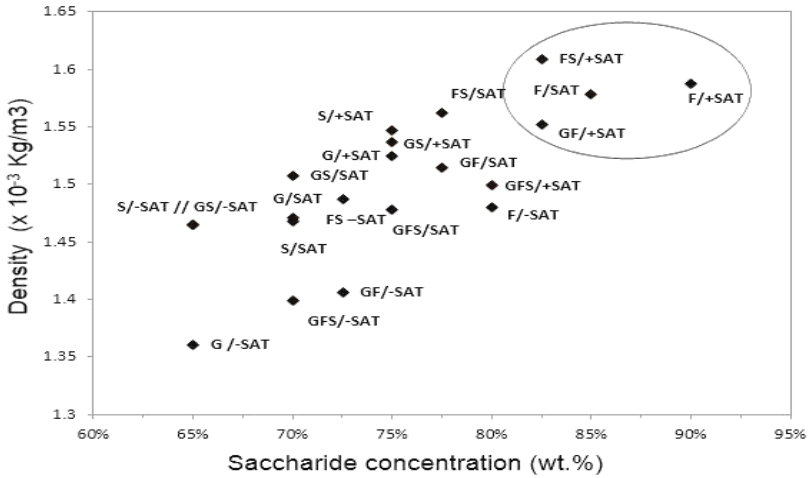

Figure 7. The density of the aqueous saccharide solutions as a function of the saccharide concentration at 50˚C. Circles indicates those solutions with improved electrospinnability (greater filament formation).

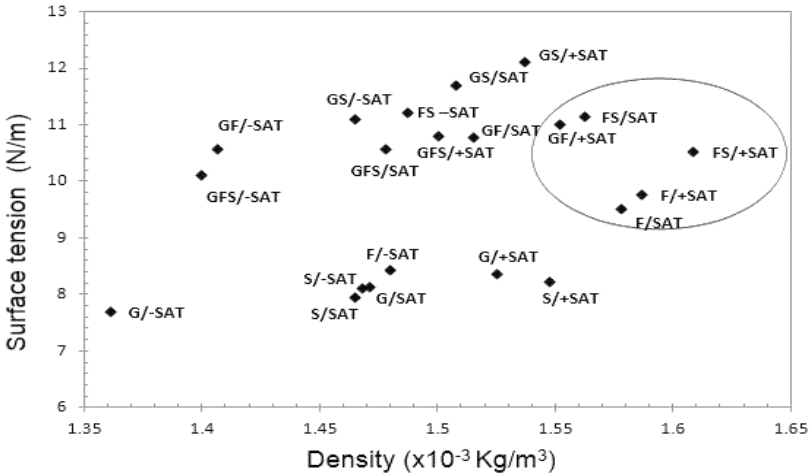

Figure 8. Surface tension as a function of density at 50˚C. Circle indicates those solutions with improved electrospinnability (greater filament formation).

For example, hydrogen bonding can have a significant effect on capillary-driven processes, such as in the cases of microfluidics and electrospinning [106-110]. Longer relaxation times of some supramolecular polymer solutions are also associated with higher visco-elasticities [10, 111]. Often, such viscoelastic behaviour could be explained by the sticky reptation model of associating networks. The sticky reptation model proposes that reversible (short-term) bonds in supramolecular polymers, such as hydrogen bonds, can act as "sticky points" for the so-called "associative supramolecular networks", and so dictate the long-term stress and strain dynamics of the bulk solution [112]. In other words, concentrated saccharide solutions could behave as an interconnected network or gel, for time scales shorter than the lifetime of these reversible bonds (e.g., hydrogen bonding) [112].

Moreover, it is known that increased filament length or extensional capacity may indicate a polymer solution with a higher elasticity [17, 113, 114-116]. The associated electrospinnability for viscoelastic polymer systems is also found on nonpolymeric systems, as supported by the relationship between higher zero-shear viscosities, longer stable jet lengths (elasticity) and electrospinnability of tested saccharide solutions (Figures 10 and 11).

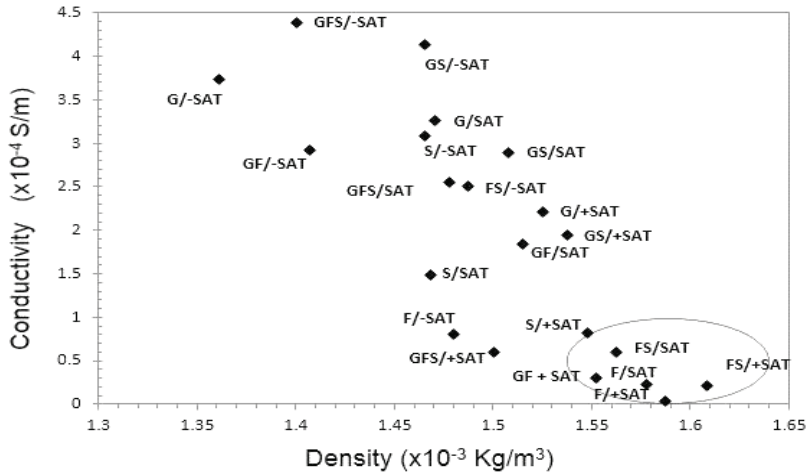

Figure 9. Conductivity as a function of density at 50 C. Circle indicates those solutions with improved electrospinnability (e.g., higher filament formation).

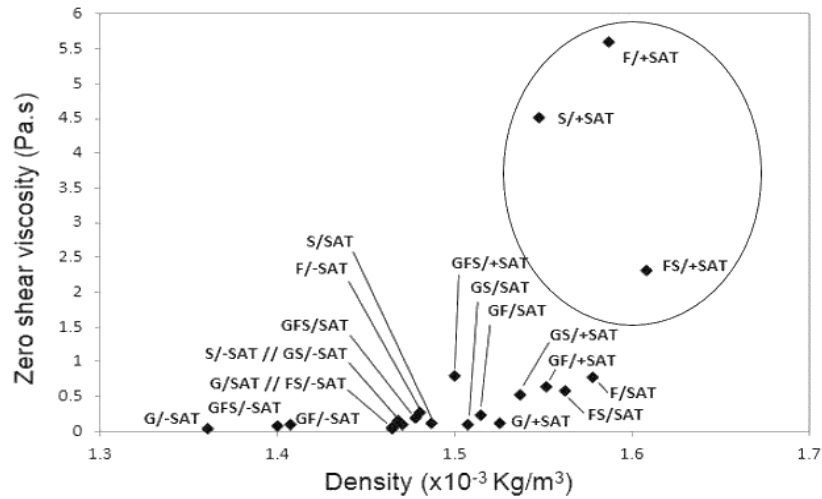

Figure 10. Zero-shear viscosity as a function of density at 50˚C. Circle indicates those solutions with improved electrospinnability (greater filament formation).

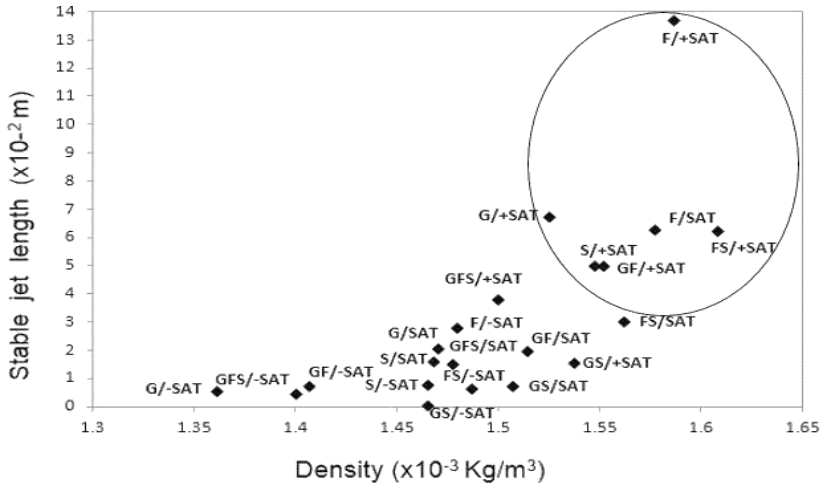

Figure 11. Stable jet length as a function of density at 50˚C. Circle indicates those solutions with improved electrospinnability (greater filament formation).

Furthermore, the elasticity of supramolecular polymers while in solution may be related to electrospinnability through gelation or colloid aggregation via hydrogen bonding networks [111, 112, 117]. Moreover, viscoelasticity also may play an important role in the electrospinnability of cyclodextrins [24, 27]. For example, Uyar et al. proposes that hydrogen bonding promotes the self-assembly of CD molecules into aggregates, resulting in solutions of higher elasticity and electrospinnability [27]. Similarly, sucrose aqueous solutions can strongly bind water molecules in its hydration sphere, orientating water molecules even at long distances, as in hydrocolloids clusters [3-5, 118].

1.3.3.2 *Viscoelasticity of saccharide solutions*

Viscosity values measured for saccharide solutions were relatively lower when compared with typical polymeric materials usually measured at 20˚C, since the associated dynamic shear viscosities for tested saccharide solutions did not exceed 10 Pa·s at 50˚C (Figure 12). Moreover, in contrast to the expectation that diluted saccharide solutions behave as Newtonian fluids, most of the fructose- and sucrose-containing concentrated solutions behaved as non-Newtonian fluids. Similarly, Quintas et al.

found that nucleation and crystal growth of metastable supersaturated sucrose aqueous solutions during shear stress do not correlate with the expected Newtonian behaviour predicted by the Arrhenius model [119]. However, no conclusive experimental evidence has been reported on the correlation between the nucleation processes of concentrated sucrose aqueous solutions during shear stresses and the viscoelasticity of the solution. Hence, the chemical bonding dynamics (nucleation) relating to the associated colloid aggregation (van der Waals) and self-assembly processes (hydrogen bonding) that influence the electrospinnability of concentrated saccharide solutions are still too complex to validate experimentally [4, 27, 101].

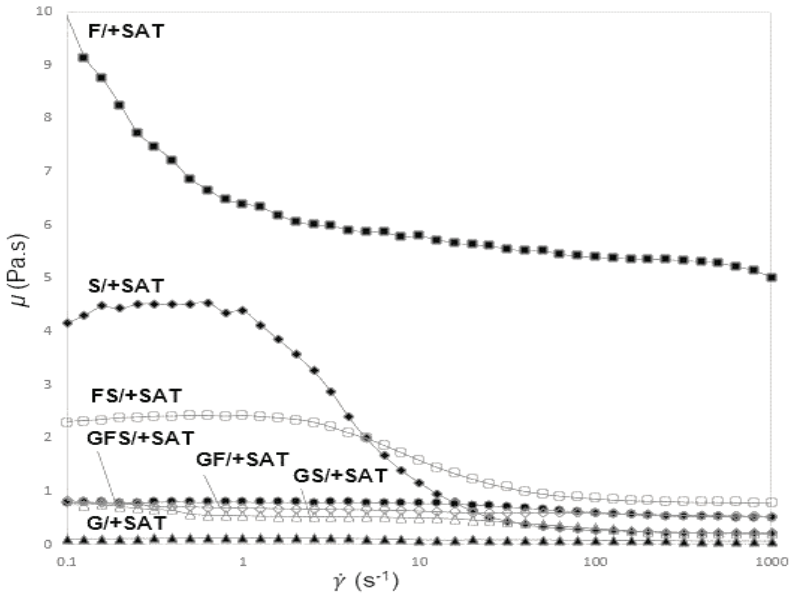

Figure 12. Shear rate ($\dot{\gamma}$) to dynamic viscosity (μ) relationship for single, binary and ternary combination of saccharide at 50˚C.

The apparent complex viscoelastic behaviour may be associated with the nonlinear additivity of hydrogen bonding and van der Waals forces when subjected to external electric fields [10, 11]. Also, the orientation of the charged solvent (ionised water) molecules may in turn be associated with a high surface density of electron-donors (reducing sugars), often related

to a net repulsive Lifshitz–van der Waals interactions between molecules [10, 11]. The non-Newtonian behaviour of the nonreducing sugars is especially noticeable for the sucrose and fructose-sucrose supersaturated solutions, as evidenced by the shear thinning behaviour of FS/+SAT (Figure 12). Also, all tested samples were more viscous than elastic due to the G' values always being lower than their respective G'' (not shown). However, S/+SAT showed the highest G' at higher angular frequencies while F/+SAT showed the lowest G' at all angular frequencies (Figure 13). Likewise, binary mixtures of sucrose solutions showed higher G' at all angular frequencies, while GF/+SAT showed the lowest G' of all solutions (Figure 13). Moreover, F/+SAT, which exhibited the longest stable jet length (Figure 11), also showed the second lowest G' of all the solutions

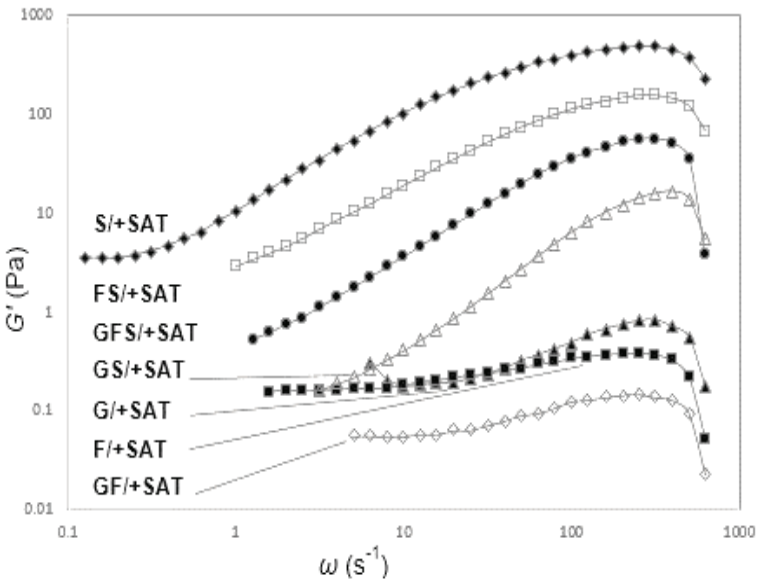

Figure 13. Angular frequency to storage modulus (G′) relationship for single, binary and ternary combination of saccharide at 50˚C.

1.3.3.3 *Electrospinnability analysis*

The stable formation of polymer fibres during electrospinning requires

greater than two entanglements per chain to provide sufficient molecular cohesion, according to the chain entanglement theory. The critical overlap concentration (c^*) may be calculated using equation 4, where M is the molecular mass, N_a is the Avogadro number, and $\langle r^2 \rangle^{3/2}$ is the root-mean-square end-to-end distance

$$c^* \approx \frac{3M}{4\pi * [(r^2)^{3/2}] * N_a} \qquad \text{equation 4}$$

Macromolecules with low molecular mass and many peripheral hydroxyl groups (e.g., high hydrophilicity) cannot be described by an end-to-end distance, due to fluctuations in their hydration shells [110]. Consequently, the use of the hydrodynamic radius (R_h) offers a more accurate representation of molecular dimensions (van der Waals radii) than the root-mean-square end-to-end distance, as given by equation 5.

$$R_h = \sum_i^n 2\left(\frac{r/n}{\sqrt{2\pi}}\right) \qquad \text{equation 5}$$

Using open source software Avogadro 2.0 as the computational method to model the van der Waals molecular ratio for each saccharide molecule, the Merck Molecular Force Field (MMFF) for sucrose, glucose, and fructose, through a standard geometry optimisation was calculated. Subsequently, an approximate hydrodynamic radius (R_h) of the glucose, fructose and sucrose molecules was determined by averaging the linear distances between each carbon and peripheral hydrogen and oxygen atom (Figure 14) [110, 114- 116]. The critical overlap concentration (c^*) was then calculated using Equation 4, and values are shown in Table 2.

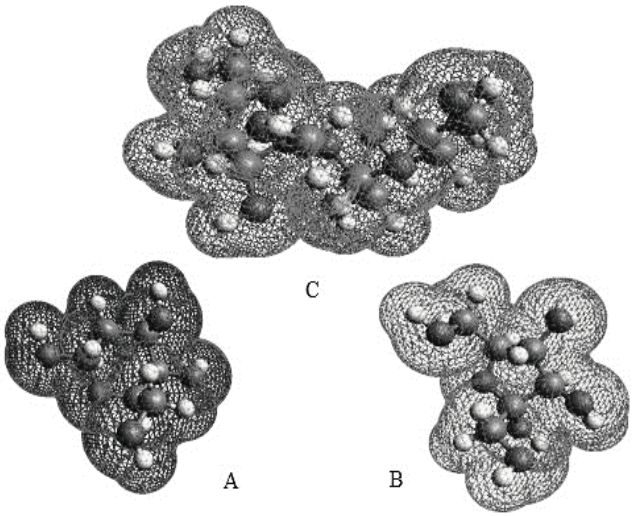

Figure 14. Molecular models showing their van der Waals molecular ratios for glucose (A), fructose (B) and sucrose (C).

Based on the presented evidence, critical concentration or chain entanglement theory applied to electrospinning does not predict the electrospinnability of tested saccharide solutions. The required critical entangled (C*e*) concentrations ($Ce \sim 10 \times c^*$) predicted by the model is one order of magnitude higher than the critical overlap concentration (c^*) found for the tested saccharide solutions (Table 2). In other words, the electrospinnability of nonpolymeric systems can be achieved with less than $2 \times c^*$ (where $Ce = 10 \times c^*$), contrasting with the chain entanglement electrospinnability condition of $2 \times Ce$.

Table 2. Critical overlap concentration values for all solutions based on the hydrodynamic radius (R_h).

Variable	**Solution**						
	G	F	S	GFS	GF	GS	FS
M **g/mol**	180	180	342	210	180	236	228
R_h **Å**	2. 5	3. 1	6. 2	3. 9	2. 8	4. 4	4. 7
c^* **wt. %**	291	151	36	90	203	72	56

In contrast, electrospinnability predicted by extensional rheology models depends on the growth of a visco-elasto-capillary wave, similar to the Rayleigh instability that scales with λ^{-1}, where λ is the characteristic polymer relaxation time [17, 120]. This corresponds to the elasto-capillary number (Ec = Wi/Ca); an increase in this number results in a strong stabilisation of the jet. Thus, the Deborah number must be greater than 1 for stable fiber formation [120]. Therefore, the following conditions must be true, Oh > 1 (viscosity) and De > 1 (elasticity), in order for a continuous non-beaded filament to be formed (Figure 2).

For example, the longest Rouse relaxation time for polymers is usually in the range of 1 to 3 s. Relaxation processes that occur on smaller time scales than 10–100 ms cannot be unambiguously resolved [120]. However, during electrospinning, molecular relaxation is usually increased with the strength of the external electric field. This effect cannot be attributed to the electro-rheological effect alone, but also to the polarisation current induced in the solution. Moreover, relaxation times for many biopolymers and supramolecular polymers with relatively small chains and a high degree of OH^- groups and/or permanent dipoles cannot usually be determined by the Rouse model. Similarly, the Rouse model holds for only up to a certain crossover time or frequency for short chain molecules in solutions over the chain entanglement concentration (e.g., colloidal aggregates).

Aggregates of small molecules measured over the higher frequencies might only move within a "tube" formed by the surrounding aggregates (hydration shells), as described by the reptation model. Hence, a simplified version of the tube model e.g., $\lambda = k(G')/k'(G'')$, was used instead of the Rouse model, for predicting the longest relaxation times of the solutions (data not shown). However, even the simplified version of the tube model did not accurately fit the predicted values over the whole range of frequencies, due to the high standard deviations at lower concentrations. Approximate values were then used to estimate the intrinsic Deborah number, and consequently calculate the non-dimensional numbers required by the elasto-visco-capillary theory, as proposed by McKinley et al., (Figure 15) [15, 16].

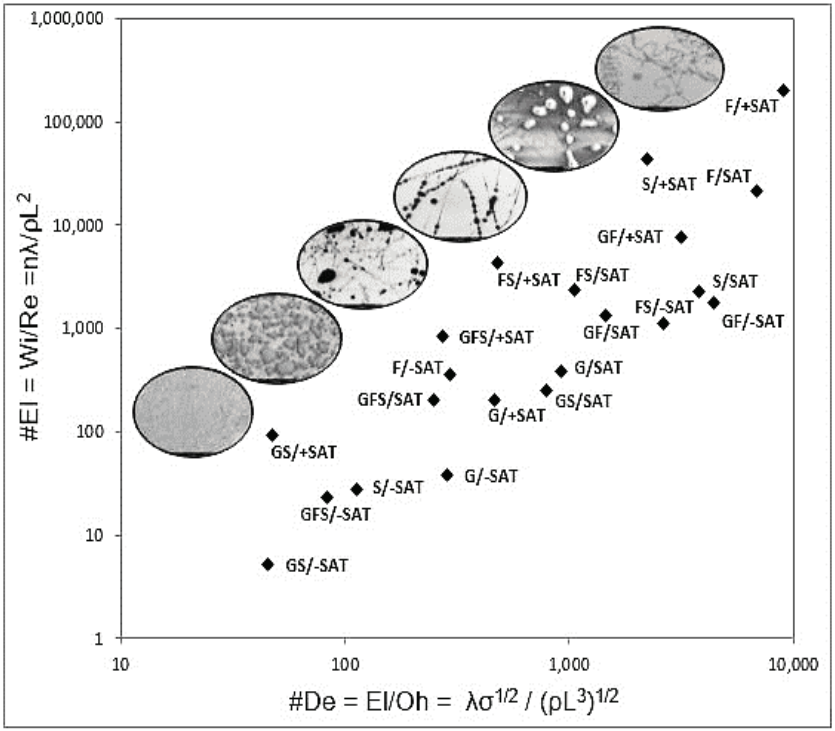

Figure 15. Logarithmic scale of the elasto-capillary numbers plotted against the intrinsic Deborah numbers for all saccharide solutions, at all concentrations at 50˚C.

However, visco-elasto-capillary theory does not offer an explanation as to how bounded water and aqueous phase separation (aggregate formation) relate to hydrogen bonding interactions and jet charge-transport mechanisms [101]. Nonetheless, visco-elasto-capillary theory suggests that longer relaxation times or the capacity to remain electrically stressed for longer periods of time, correlates to higher electroviscoelasticity, resulting in improved electrospinnability.

Modified sucrose solutions (e.g., octa-*O*-acetyl sucrose and octa-*O*-methyl sucrose), with different hydrogen bonding capacities and molecular polarities, were electrospun to further investigate secondary bonding and electrospinning process relationships.

1.3.4 Octa-Acetyl/-Methyl Sucrose

The significance of intermolecular forces on the electrospinnability of modified sucrose derivatives (e.g. octa-*O*-acetyl sucrose and octa-*O*-methyl sucrose) using an aqueous solution of sucrose as the control, was investigated. Octa-*O*-acetyl sucrose has been used as enzymatic catalysis additive for selective hydrolysis in some lipases [126, 127]. In comparison, octa-*O*-methyl sucrose is commonly used as non-crosslinking agent for polymer synthesis [128]. In this study, octa-*O*-acetyl sucrose and octa-*O*-methyl sucrose were used as test materials for evaluating the significance of hydrogen bonding and van der Waals forces in the electrospinnability of saccharide solutions. Neither compound has the capacity to donate hydrogen with nearby solvent molecules. Whereas, sucrose has the capacity to accept and donate hydrogen to other solvent molecules like water.

Both, octa-*O*-acetyl sucrose and octa-*O*-methyl sucrose are only capable of acting as H-bond acceptors (e.g. from solvent molecules such as water), since neither compound has any hydroxyl groups (Figure 16). Therefore neither octa-*O*-acetyl sucrose nor octa-*O*-methyl sucrose can participate in intermolecular reciprocal hydrogen-bonding interactions with other molecules of the solute. Moreover, octa-*O*-methyl sucrose ($C_{20}H_{38}O_{11}$, 454.51 gr/mol) has 33% more mass than sucrose ($C_{12}H_{22}O_{11}$, 342.11 gr/mol), while octa-*O*-acetyl sucrose ($C_{28}H_{38}O_{19}$, 678.60 gr/mol) has 98% more mass.

Likewise, the hydrogen bond acceptor sites (oxygens) for octa-*O*-methyl sucrose (eleven) are equivalent to the number of oxygens in sucrose (eleven) but 40% less than octa-*O*-acetyl sucrose (nineteen). However, the rotatable bond sites of octa-*O*-methyl sucrose (thirteen), are less than the rotatable bond sites octa-*O*-acetyl (twenty-one) both greater than the rotatable bond sites of sucrose (five), (Figure 16). The fact that octa-*O*-acetyl sucrose is more polar than octa-*O*-methyl sucrose yet neither has the capacity for reciprocal intermolecular H-bonding, offers the possibility to test the significance of van der Waals forces (dipolar moment dynamics) in the electrospinnability of saccharide materials (Table 2).

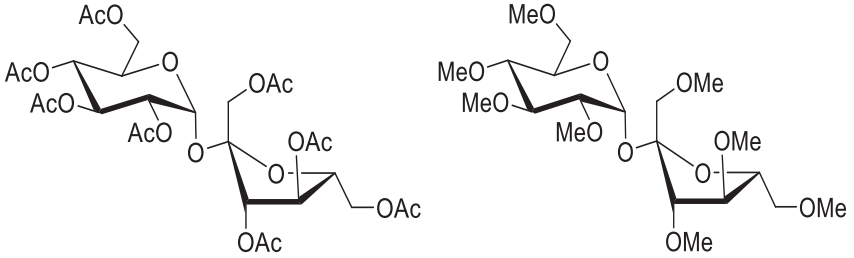

Figure 16. Octa-*O*-acetyl sucrose (right) and Octa-*O*-methyl sucrose (left).

Concentrations of 75 wt. % sucrose, octa-*O*-methyl sucrose and octa-*O*-acetyl sucrose in deionised water for all three solutions were used. The aqueous solutions were prepared by using a water bath at a temperature of 50 ± 2 °C until complete solute dissolution was achieved. Subsequently, samples were stored at 50 ± 2 °C to avoid precipitation of the concentrated sugars. The n-octanol / water partition coefficients (cLogP) for sucrose (-3.7), octa-acetyl sucrose (-0.9) and octa-methyl sucrose (-1.2) were approximated (± 0.25) using Chemdraw (Table 3). The solution of octa-*O*-acetyl sucrose had the highest pH value and the lowest conductivities of all the solutions investigated (Table 2). In contrast, the solution of octa-*O*-methyl sucrose had the lowest pH value and the lowest surface tension value of all the solutions. Sucrose (the control) had the highest surface tension and conductivity of all the samples. However, octa-*O*-acetyl sucrose showed the best electrospinnability (continuous filament formation) of all the samples tested (Figure 17).

Table 2. Physical-chemical properties of modified sucrose solutions and control.

Material	pH	Conductivity ($x10^{-4}$ S/m)	Surface tension (N/m)	Density (kg/m^3)	Partition coefficient	Hydrogen bonding capacity
Octa-*O*-acetyl sucrose	6.75	0.01	4.52	1.21×10^3	-0.9	Acceptor
Octa-*O*-methyl sucrose	4.88	0.15	2.78	1.03×10^3	-1.2	Acceptor
Sucrose	5.07	0.82	8.21	1.55×10^3	-3.7	Acceptor / Donor

1.3.4.1 *Octa-O-acetyl/-methyl sucrose electrospinnability.*

Octa-*O*-acetyl sucrose showed an improved electrospinnability as compared with sucrose. In contrast, octa-*O*-methyl sucrose solutions did not present any filament formation during electrospinning; rather electrospraying of droplets was observed. Interestingly, the aqueous sucrose solution presented both filament and droplet formation (*e.g.,* both electrospinning and electrospraying) simultaneously (Figure 17).

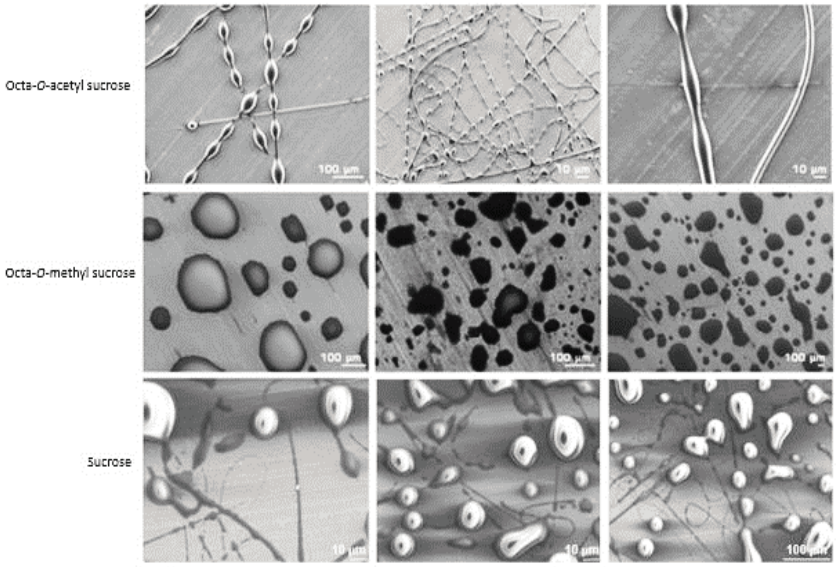

Figure 17. Scanning electron micrographs of octa-O-acetyl sucrose and octa-O-methyl sucrose in comparison to the control, sucrose; all at 75 w.t % and produced by electrospinning at 50˚C.

The fact that the per-acetylated sucrose solution did electrospin, negates the argument that reciprocal intermolecular H-bonding between solute molecules is absolutely required for electrospinnability. Also, there is a correlation between high pH, low conductivity and a low cLogP (e.g., a high molecular polarity) to the electrospinnability of the octa-*O*-acetyl sucrose. Nonetheless, the fact that sucrose also presented filament formation (to a lesser extent than octa-*O*-acetyl sucrose), suggests that hydrogen bonding, like van der Waals forces, are both required for the electrospinnability of saccharide materials.

1.3.5 Hydroxypropyl-***β***-cyclodextrin (HP-***β***-CD)

Aqueous electrospinning solutions were formulated with the intention of either enhancing (Hb-E) or disrupting (Hb-D) the overall hydrogen bonding networks between CD and solvent molecules. Hence two different solutions were made, a saturated urea solution, aimed at negatively disrupting the hydrogen bonding networks between CD and water molecules (Hb-D), and a diluted sodium bicarbonate ($NaHCO_3$) aqueous solution on a (50:50) acetone/ethanol solvent system, aimed at positively enhancing the overall hydrogen bonding network between CD and water molecules, while promoting solvent evaporation during electrospinning (Hb-E). The composition of the Hb-E solvent system was 0.5 wt. % sodium bicarbonate in 43.25 wt. % water, with 30 wt. % acetone, 20 wt. % ethanol, and 6.25 wt. % hydrogen peroxide, while Hb-D was prepared as a saturated solution of urea in deionised water. The electrospinning solutions were prepared by dispersing 2HP-*β*-CD (55–70 g/cm^{-3}) in the solvents at a temperature of 50°C ± 2°C.

1.3.5.1 *Physical-chemical properties of 2HP-β-CD solutions*

As expected, the 2HP-*β*-CD/Hb-E solutions exhibited both higher pH (Figure 18) and conductivity (Figure 19) compared with those of the 2HP-*β*-CD/Hb-D or 2HP-*β*-CD/H_2O solutions, due to the presence of bicarbonate salts. In contrast, the surface tension of the 2HP-*β*-CD/Hb-E and 2HP-*β*-CD/H_2O solutions were lower than that of 2HP-*β*-CD/Hb-D (Figure 20). The pH of the 2HP-*β*-CD/Hb-E solutions was higher than all other samples, as expected with the addition of bicarbonate salts. However, all pH values converged to a value of 9.5 with a CD concentration of 70 wt. % (Figure 18). Such linear behavior could be related to the concentration dependency of the hydronium ions' (H_3O^+) mobility while in aqueous solution. In contrast, surface tension for all solutions showed the opposite behaviour, such that surface tension values diverged with increasing concentration of cyclodextrins. For instance, all of the 55 wt. % CD solutions exhibited surface tension values of ~6 to 6.5 N/m, while the value for 75 w.t % CD solutions was 6 to 7.5 N/m (Figure 20). Similar to the case of pH, the linear effects might be attributable to the concentration dependency of added ionic salts and volatile solvent systems in contact with air. Interestingly, visco-elasto-capillary effects show that an electrospinnable system will tend to minimise its total

surface tension to form continuous filaments [15, 16]. For example, 2HP-*β*-CD/Hb-E solutions showed the lowest surface tension values of all samples yet good electrospinnability (Figure 21). Furthermore, 2HP-*β*-CD/Hb-E solutions at lower CD concentrations showed a relatively high electrical conductivity (Figure 19) but poor electrospinnability (Figure 21).

In contrast, 2HP-*β*-CD/Hb-D solutions did not electrospin into fibres, in spite of a higher conductivity compared to that of the 2HP-*β*-CD/H_2O solutions. The electrospinnability of polymeric systems is known to be related to the increased conductivity of the solution [129-134]. In the present work, a consistent correlation between the conductivity of the CD solutions (Figure 19) and resulting solution electrospinnability was not observed (Figure 21). Therefore, it appears that the conductivity of tested solutions cannot be directly linked to the electrospinnability of 2HP-*β*-CD (Figure 19 and 20).

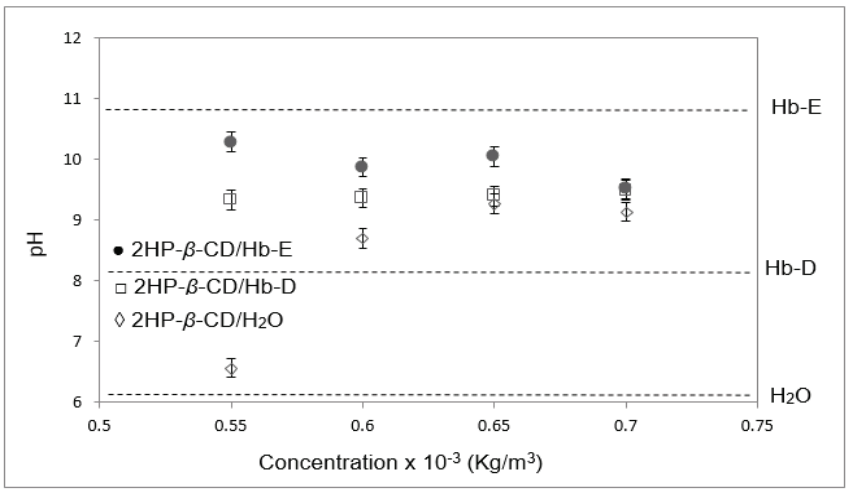

Figure 18. The pH of the 2HP-β-CD solutions as a function of solution type and concentration of 2HP-β-CD (error bars showing an average standard deviation of 0.16).

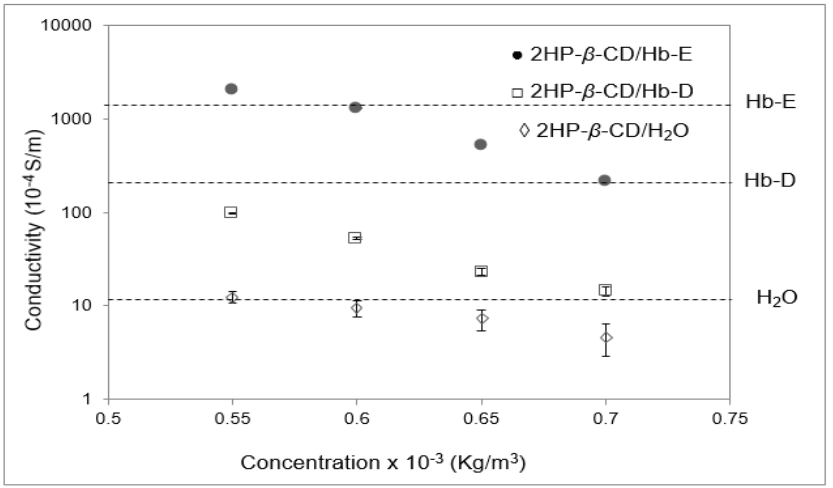

Figure 19. Conductivity of the 2HP-β-CD solutions as a function of solution type and concentration of 2HP-β-CD (error bars showing an average standard deviation of 0.86).

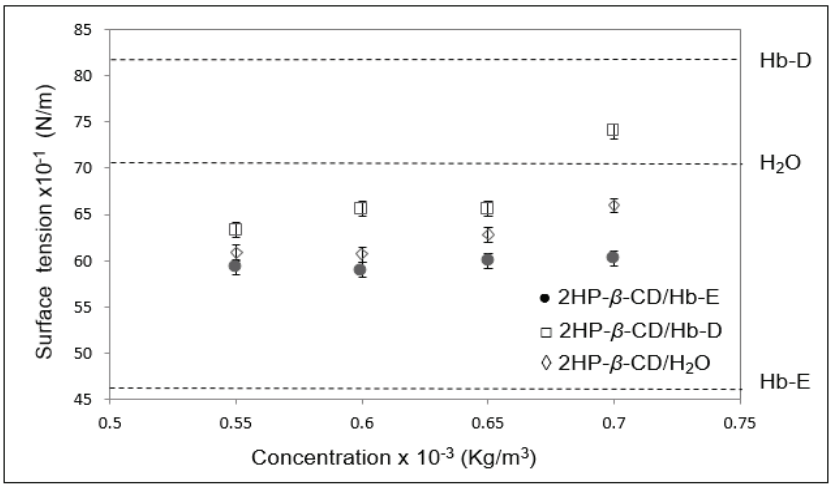

Figure 20. Surface tension of the 2HP-β-CD solutions as a function of solution type and concentration of 2HP-β-CD (error bars showing an average standard deviation of 0.41).

1.3.5.2 *Electrospinnability of 2HP-β-CD solutions*

Both stable and chaotic jet formation was observed for all 2HP-β-CD/H_2O and 2HP-β-CD/Hb-E 60 wt. % solutions. In contrast, electrospraying of droplets occurred for all 2HP-β-CD/Hb-D solutions, with no jet formation observed (Figure 21C, F, I and L). Consequently, all 2HP-β-CD/Hb-D solutions did not present any fiber formation. The electrospinning of 2HP-β-CD/H_2O solutions at concentrations of 55 wt. % and 60 wt. % resulted in electrospraying of droplets and bead-on-string structures, respectively (Figure 21A, and D). However, 2HP-β-CD/H_2O exhibited beaded morphology and stable fiber formation at concentrations greater than 65 wt. % 2HP-β-CD.

Interestingly, the electrospinning of 2HP-β-CD/Hb-E at concentrations of 60 wt. % and 65 wt. % resulted in fibres that fractured following deposition onto the collector (Figure 21E, and F). The presence of fractured fibres may indicate differential shrinkage following deposition, possibly due to a lack of crystallinity within the CD nanofibre, as the amorphous composition of electrospun cyclodextrin nanofibres has been already reported by Celebioglu and Uyar [32, 122].

The experimental data presented in this chapter further supports previous evidence reported by Uyar et al., in respect to the addition of urea salts to aqueous 2HP-β-CD solutions to deter hydrogen bonding within the solvent molecules and subsequent electrospinnability [53- 55]. Hydrodynamic radiuses of 2HP-β-CD molecules reported in literature, spanned from 0.65 nm inner diameter to 1.5 nm outer diameter, per CD molecule [135]. Critical concentration theory values using reported molecular dimensions, do not adequately predict the electrospinnability of tested materials, as concentration over 100 wt.% of solute would be required in order for 2HP-β-CD/H_2O solutions to be electrospun. Also, visco-elasto-capillary theory could not be applied to the electrospinning of CDs in modified solvent systems, due to the complex rheological properties of tested solutions during electrospinning (Figures 22 and 23). Moreover, linear viscoelasticity could not be directly related to the hydrogen bonding within the solutions, since the condition of $G' > G''$ could not be consistently related to the electrospinnability of the solutions as exemplified by 2HP-β-CD/Hb-D (Figure 23).

However, the observed viscoelastic behaviour agrees in principle with the

visco-elasto-capillary thinning theory of complex fluids; as non-Newtonian fluids with shear thinning viscosity and $G' > G''$ at higher angular frequencies are able to better resist extensional capillary thinning and filament break-up when compared with Newtonian fluids for which $G' < G''$ at low angular frequencies [151, 15]. Interestingly, no electrospinnability was observed for 65 and 70 wt. % 2HP-β-CD/Hb-D solutions, even with $G' > G''$. Also, 65 and 70 wt. % 2HP-β-CD/Hb-D corresponded to the highest surface tension values for all solutions at such concentrations, as well as showing similar conductivity and pH values in respect to 2HP-β-CD/H_2O solutions at the same concentration range. Therefore, the fact that 60 wt. % 2HP-β-CD/Hb-E shows electrospinnability ($G' > G''$), in contrast to the 2HP-β-CD/H_2O solutions at the same concentrations with $G' > G''$, suggests that the Hb-E solvent system had a positive impact on intermolecular interactions and consequent aggregate formation (electrospinnability) in comparison to water systems.

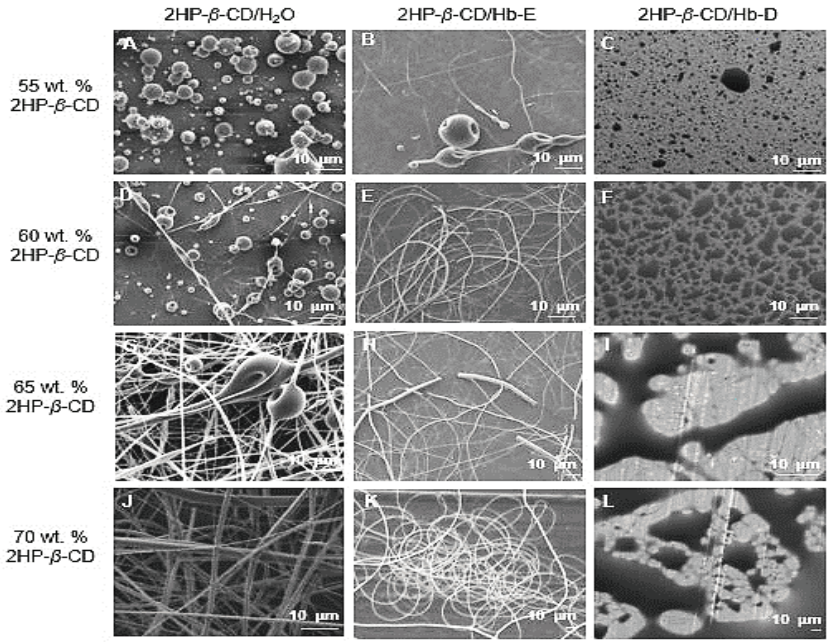

Figure 21. Scanning electron micrographs of as-deposited electrospun 2HP-β-CD samples as a function of CD concentration and solvent type produced by electrospinning at 50˚C.

1.3.5.3 *Viscoelasticity of 2HP-β-CD solutions*

Rheological measurements were used to compare the viscoelastic relationships between the electrospinnability of the 2HP-β-CD solutions of varying solvent systems. Shear thinning behaviour was observed as a decrease in the dynamic viscosity (μ) with increasing shear rate ($\dot{\gamma}$). Shear thinning was observed for all solutions during rotational testing (Figures 22A, B and C). The frequency response of the 2HP-β-CD solutions showed that solutions exhibit predominantly elastic behaviour over the angular frequency (ω) range investigated, as indicated by a storage modulus (G') at least an order of magnitude higher than the loss modulus (G'') (Figures 23A, B and C). In general, 2HP-β-CD solutions exhibited weakly elastic behaviour above 65 wt. % 2HP-β-CD.

The storage (G') and loss (G'') modulus of 75% wt. % 2HP-β-CD (10^4–10^6 Pa) was in agreement with that for native β-CD at 150% (w/v) as reported in the literature (Figure 23) [122]. In contrast, the viscosity of native β-CD, as reported in the literature [122], ranged between two to three orders of magnitude below that obtained for 2HP-β-CD/H_2O and 2HP-β-CD/Hb-E solutions. Discrepancies with the reported literature values may be attributed to the difference in the molecular weight of the β-CD derivative used in this work (2HP-β-CD) (1460 g/mol) [53].

The difference in the molecular weight could also correspond to the variance in the reported viscosity (Figure 22) [53]. Also, a relatively high molecular substitution per anhydrous glucose unit (0.57–1.29) is reported in this work in comparison with data from available literature (0.6–0.9) [122]. Consequently, correlations with present experimental results are not possible due to the lack of published β-CD density and molecular weight values elsewhere in the electrospinning literature [27, 32, 53, 122].

Furthermore, the viscosities of 2HP-β-CD/H_2O at 65 and 70 wt. % CD were five orders of magnitude higher than those for 55 and 60 wt. % 2HP-β-CD. The large difference in viscosity suggests a pronounced increase in intermolecular interactions between the CD molecules above 60 wt. % 2HP-β-CD. Similarly, 2HP-β-CD/H_2O exhibited elastic behaviour where G' is significantly higher than G'' for all CD concentrations (Figure 23A).

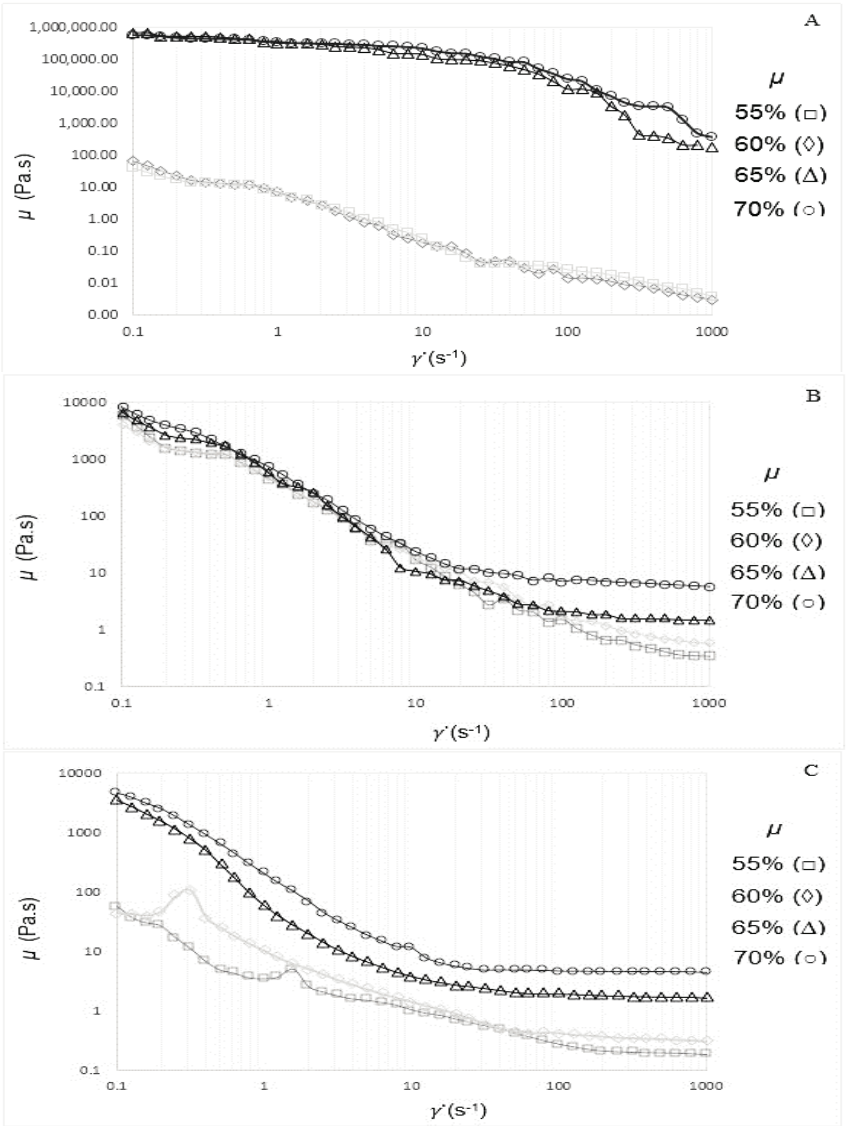

Figure 22. The dynamic viscosity as a function of the shear rate and 2HP-β-CD concentration at 50°C; for (A) 2HP-β-CD/H2O, (B) 2HP-β-CD/Hb-E and (C) 2HP-β-CD/Hb-D.

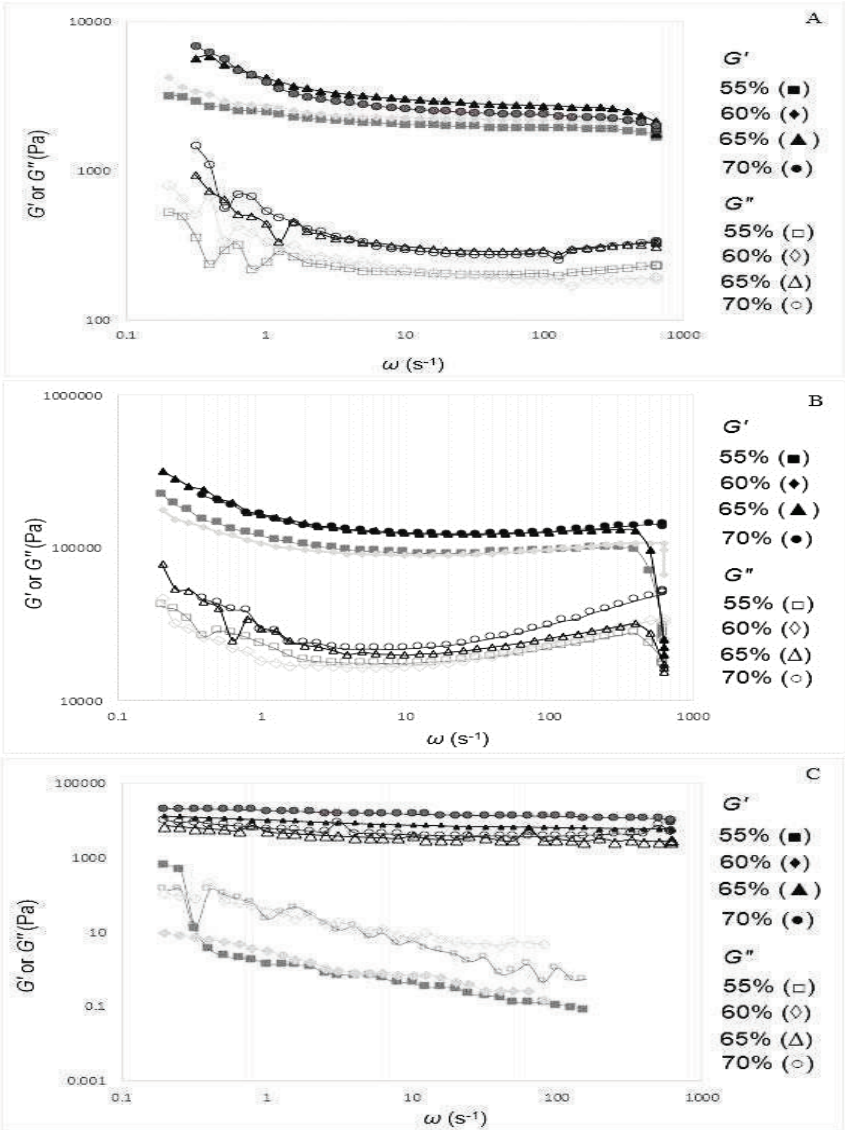

Figure 23. The storage and loss modulus as a function of the angular frequency and 2HP-β-CD concentration at 50°C; for (A) 2HP-β-CD/H2O, (B) 2HP-β-CD/Hb-E and (C) 2HP-β-CD/Hb-D.

In contrast, 2HP-β-CD/Hb-D solutions showed lower values of G' and G'' at low concentrations (55–60 wt. % CD) compared with higher CD concentrations for 2HP-β-CD/Hb-D solutions (Figure 22). Moreover, Hb-D based solutions with 65 or 70 wt. % 2HP-β-CD could not be electrospun into fibres even though $G' > G''$. In contrast, 2HP-β-CD/H_2O solutions showing $G' > G''$ could be electrospun into fibres. The 60 wt. % 2HP-β-CD/H_2O solution exhibited poor electrospinnability compared with a 60 wt. % 2HP-β-CD/Hb-E solution that exhibited similar viscoelastic behaviour ($G' > G''$) (Figure 21D and E). However, electrospinnability was not observed for any 2HP-β-CD/Hb-D solutions, regardless of $G' > G''$ at higher CD concentrations (Figure 23). Similarly, 2HP-β-CD/Hb-E samples exhibited $G' > G''$ for all 2HP-β-CD concentrations; however, electrospinnability was not observed for 55 wt. % 2HP-β-CD/Hb-E (Figure 23).

Additionally, the development of a plateau in G' over a wide range of angular frequencies suggests that the presence of 2HP-β-CD aggregates resulted in gel-like behaviour for all solutions. The nonlinear viscoelastic behaviour observed in the solutions is typically associated with a high number of associating networks, such as those described by the sticky reptation model proposed by Rubinstein et al. [112]. Furthermore, a G'-G'' crossover point could not be observed, creating a practical limitation in calculating the molecular relaxation time using rheometry. Thus, Rousse relaxation times of the solutions were not detectable over the range of frequencies investigated.

Likewise, the sticky reptation model of associating networks proposes that rapidly reversible (short-term) bonds in supramolecular polymers, such as hydrogen bonds, can act as sticky points to form associative supramolecular networks that dictate the long-term stress and strain dynamics of the bulk solution [112]. Thus, the solution is capable of behaving as an interconnected network on time scales shorter than the lifetime of the reversible bonds. Moreover, dielectric or light scattering spectroscopy has shown that the oxygen atoms in a saturated aqueous CD solution could act as "open-close" stickers [31, 35, 36], where there are noticeable differences between α-, β- and γ-cyclodextrin (CDs) [136]. Nevertheless, hydrogen bonding donor mechanisms might not necessarily be related to electrospinnability, as shown by the electrospinning of octa-acetyl-sucrose.

Additionally, the gel-like behaviour of cyclodextrin-based solutions is in agreement with the literature reports on nonlinear viscoelasticity or solid-like behaviour for CD solutions, possibly due to complex intermolecular hydrogen bonding [27, 32, 53, 57-59]. Evidence suggests that 2HP-β-CD/Hb-D solutions can still form aggregates with themselves and bounded water in the presence of urea, possibly due to steric effects, as evidenced by their viscoelastic behaviour ($G' > G''$) at higher 2HP-β-CD concentrations. However, the significance of van der Waals forces versus hydrogen bonding networks during electrospinning, is not yet fully understood.

1.3.6 Glucose syrup

The electrospinnability of food-grade glucose syrup, as carrier bio-material for mānuka oils, was investigated in order to provide affordable honey nanofibre formulations for both air filtration and skincare applications. However, as food-grade glucose syrup contained added preservatives, the composition of the syrup was investigated by Mass spectrometry and HPLC; in order to determine the purity of the material. In order to provide mechanical and bioactive properties to the nanofibre membranes, a concentrated aqueous mānuka-saccharide solution in combination with proprietary polymer and non-hydrolyzed marine collagen formulations, was used to manufacture the facemasks and skincare patches, respectively.

1.3.6.1 *Experimental procedures and results*

A culinary-grade glucose syrup was used as received for the electrospinning experiments (Queen Fine Foods Ltd., Brisbane, Australia). The syrup is a glucose extract derived from maize that contains traces of sulfur dioxide (preservative 220) and sodium sulphite salts (80–150 mg/kg max.). Hence, the composition of glucose syrup was studied by HPLC and Mass spectrometry, to discard electrospinnability by the presence of polymeric materials. Also, the glucose syrup viscosity was too high for it to flow through the electrospinning capillary, therefore a 75% wt. glucose syrup concentration in 15% wt. water was used (Table 3).

Table 3. Physical properties of the glucose syrup at 25°C.

Property	Value
Concentration	75% wt. % syrup/H_2O
Surface tension	98.11 mN/m
Conductivity	1.5 μS/cm
pH	5.5
Density	1.5 g/mL
Zero-shear viscosity	38,600 Pa·s

A possible mechanism for the electrospinnability of the glucose syrup systems could rest upon the ability of mutarotation on the anomeric carbon within the pyranose-glucose ring, which yields the two distinct stereoisomer configurations of glucose (α and β) [3, 137]. This mutarotation process could often produce metastable dihexoses through 1, 6 glycosidic bonds [5, 6].

Saturated solutions of saccharide mixtures could also yield more complex metastable molecular architectures after heat and electrical processing. Furthermore, oligosaccharides and other more complex molecular architectures, possibly reacting with added preservatives could have been produced during the electrospinning of glucose syrup.

However, mass spectrometry (Figure 24) and HPLC (Figure 25) confirmed that the tested glucose syrup was mainly composed of monosaccharide (glucose and fructose [$C_6H_{12}O_6$]), disaccharide (sucrose and maltose [$C_{12}H_{22}O_{11}$]), and trisaccharide (raffinose [$C_{18}H_{32}O_{16}$]). Evidence of possible chemical modifications (covalent bonding) on the saccharide solutions and saccharide electrospun material remains to be found (Figure 24 and 25).

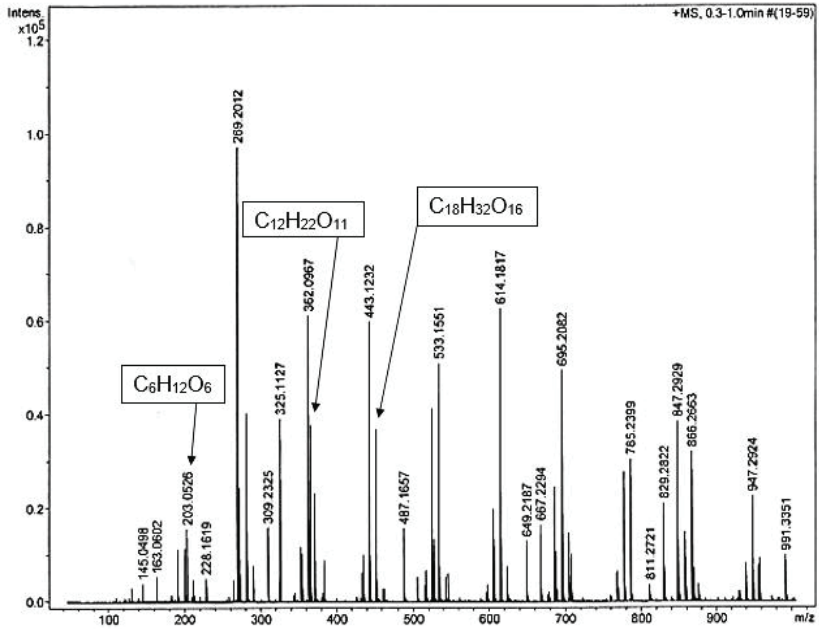

Figure 24. Mass spectrum from MS showing the intensity (y-axis) as a function of the mass-to-charge ratio (x-axis). The presence of the isomers of glucose, sucrose and raffinose are indicated at mass-to-charge ratios of 203.05, 365.1 and 527.16, respectively.

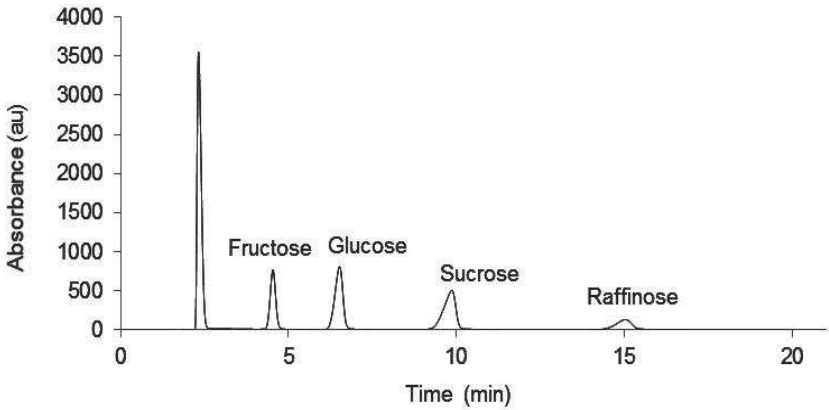

Figure 25. HPLC chromatogram confirming the presence of fructose, glucose, sucrose and raffinose in the glucose syrup. The first peak is the injection peak.

1.3.6.2 *Glucose syrup electrospinnability*

Typical electrospinning behaviour was observed for the glucose syrup, consisting of stable and chaotic jet formation (Figure 26). These photographs show the heaviest parts of the electrospun jet as dark beads, within the spinning cone. The polarity of the applied voltage did not influence the electrospinning behaviour of the glucose syrup, hence positive polarity was used throughout the experimentation.

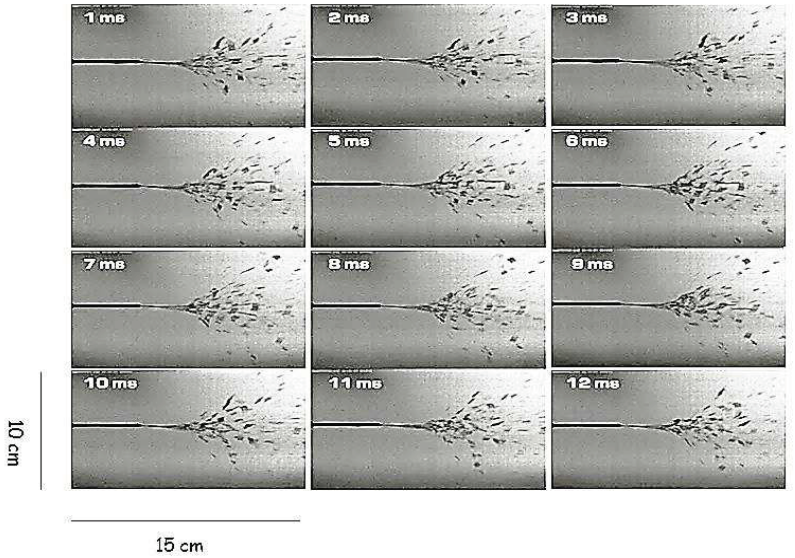

Figure 26. Series of high-speed photographs taken at 1000 fps during the electrospinning of the glucose syrup.

Published results for the results shown in Figure 26 and 27, demonstrate for the first time that food-grade glucose syrup can form continuous filaments during electrospinning [101]. Also, the highly-beaded structures of the filaments (Figure 6.5C and 6.5D) further support the viscoelastic behaviour of the material.

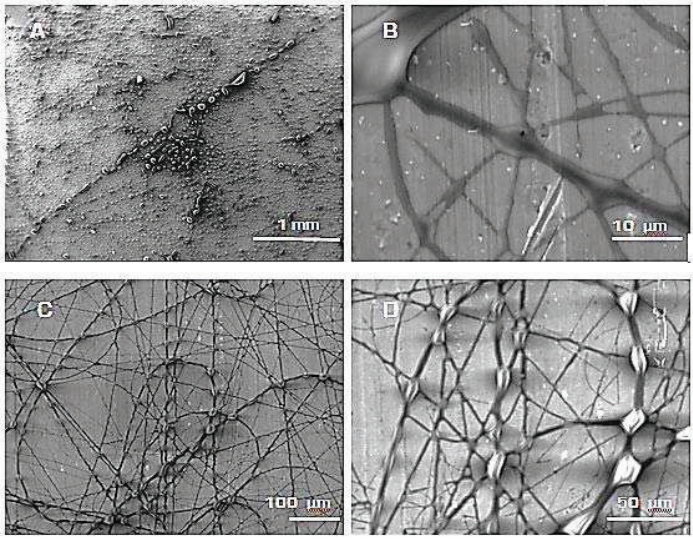

Figure 27. SEM images of electrospun glucose syrup at varying magnifications.

1.3.6.3 *Mānuka honey nanofibre media*

Commercially available mānuka honey did not show electrospinnability, mostly due to the high water and suspended solids concentration (>20%). Subsequently, a formulation based on the syrup replica containing mānuka oils, was designed to carry the antimicrobial mānuka bio-actives, as well as to improve nanofibre adhesion between substrate layers. Hence, a mānuka-syrup-collagen and a mānuka-syrup-polymer nanofibre composite, were developed for skincare patches and air filtration facemasks respectively. Although both prototypes used mānuka oils and glucose syrup (Figure 28), the properties of the electrospun nanofibres were completely different (hydrophilic versus hydrophobic), due to the combination with other materials (marine collagen and polymethyl methacrylate - PMMA).

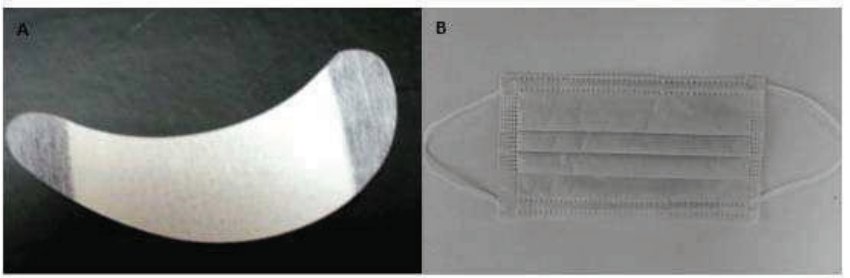

Figure 28. Prototypes of the honey–nanofibre composite media for cosmetic patches (A) and antimicrobial facemasks (B).

1.3.6.4 *Air filtration facemasks*

Air filtration markets are becoming an increasingly competitive market, with many new technological developments being commercialised across different air filtration sectors (e.g., antipollution facemasks, air purifiers, HVAC, etc.), especially in China [138-140]. There are many social and economic circumstances contributing to human health problems, for example low-income urbanites breathe 28% more noxious particulate matter (PM2.5) than residents in high-income areas [141,142]. High-efficiency microfibre respirators currently available in the market are usually sold at prices ranging from 15 to 35 USD per item, whereas the Chinese minimum wage per day is approximately 23 USD [143, 144]. Furthermore, high breathability (low pressure drop or ΔP) at high-filtration efficiencies is the main design parameter for the development of facemasks [138]. Microfibre media can often achieve high efficiencies only at low breathability (high pressure drop) [145, 146, 141,142]. In contrast, nanofiber media can achieve both: high efficiency and high breathability [145-149]. Moreover, the ability to integrate active ingredients (e.g., mānuka oils) into the media is a clear competitive advantage of nanofiber technology versus standard microfibre processing methods [149-151]. The air filtration facemasks prototype developed used several layers of the composite nanofibre material deposited onto a nonwoven polypropylene microfiber substrate, until a density of 1 gram per square meter (1 gsm) was obtained (Figure 29). The composite nanofibre nonwoven medium was then sandwiched between polypropylene substrates and cut to specific roll dimensions. Subsequently, manufactured media was sent to China for processing at an industrial facemask-manufacturing facility (Figure 28B).

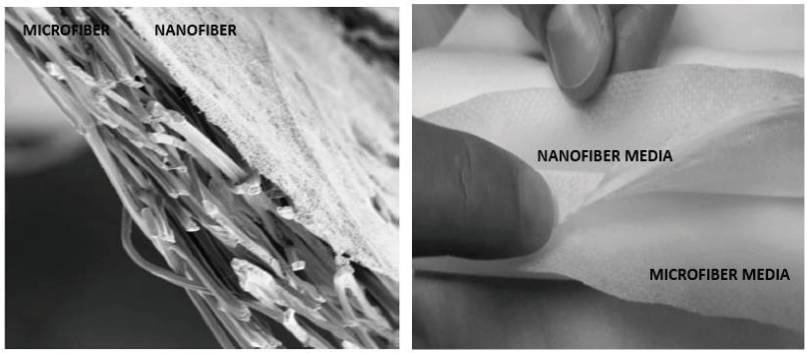

Figure 29. A mānuka–glucose syrup/ polymer composite, electrospun nanofibre layer (1 gsm), sandwiched in between two polypropylene substrates.

1.3.6.5 *Skincare patches*

The ActiVLayr™ skin delivery platform is a patented technology (WO/2013/0350720), based on the denatured whole chains of type 1 collagen extracted from NZ hoki fish skins [152]. The type 1 collagen used to produce ActiVLayr™ is highly hydrophilic, because the relatively high content of hydroxyproline in the hoki skins promotes hydrogen bonding networks between the triple helix structure of the collagen [152, 153]. Moreover, this particular source of collagen does not need to be hydrolysed to be processed at room temperature, like most collagens in the market, since the internal triple helix structure is in reversible kinetic-thermal equilibrium at standard ambient conditions [154]. ActiVLayr™ patches are usually commercialized using a wide range of plant and fruit extracts derived from the waste stream of the New Zealand wine and food industries. The ecologically sourced extracts contain a wide range of polyphenols, catechins, vitamins, flavonoids, and others. However, as increasing market demand for mānuka oils, kānuka honey and bee venom products continues to rise in Asia, new formulations based on such materials are highly needed in order for ActiVLayr™ patches to continue to be commercially profitable.

The skincare prototype patch co-developed as part of this thesis used a proprietary combination of saccharides (based on the glucose syrup replica formulation), denatured whole chains of collagen and mānuka oils (Figure 30).

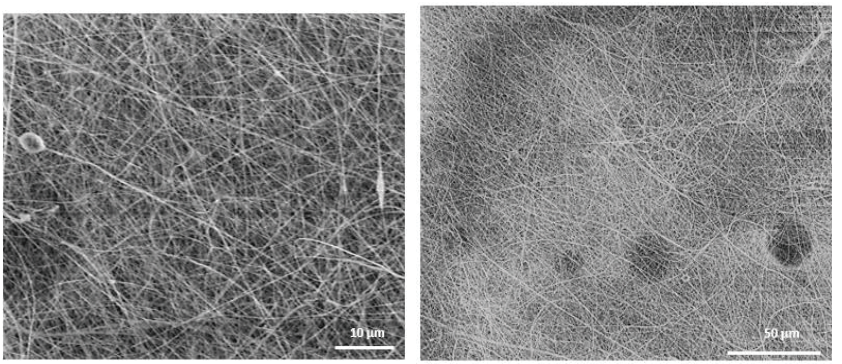

Figure 30. Scanning electron micrograph of the mānuka-syrup-collagen nanofibre composite

1.4 DISCUSSIONS AND CONCLUSIONS

Determining the electrospinnability of a given material is a complex problem that involves the consideration of many different solution and process parameters. The additivity of all intermolecular forces is far from straightforward since different types of force decay with distance at different rates, and according to different laws. For example, van der Waals and hydrogen bonds are much weaker than covalent bonds, with typical energies of 10–50 kJ/mol and bond lengths of 0.3–0.4 nm [110]. Also, van der Waals forces, which can be catalogued into three different sub-classifications (Keesom, Debye and London forces), obey similar linking rules. However, in combination, the interactions between these forces can result in completely different behaviours from the predictions expected from the same primary force (van der Waals equations) [110, 105].

For example, the electrospinnability of 2-hydroxypropyl–β cyclodextrins (β-hCD), in both hydrogen bonding enhancing and hydrogen bonding disrupting solvent systems, clearly showed that electrospinning of supramolecular materials is heavily dependent on intermolecular bonding mechanisms, e.g., hydrogen bonding. Also, the nonlinear viscoelasticity (gelation) of tested CD solutions further supports the proposition that high-density hydrogen bonding networks might be produced when there is an increment in the degree of hydration (bound water) per CD molecule [31, 35]. Furthermore, networks of hydrogen

bonds can show the phenomenon of cooperativity, leading to deviations from reciprocal (acceptor/donor) additivity of standard hydrogen bond properties [110]. Moreover, hydrogen bonds could induce dipolar moments through van der Waals mechanisms across the molecular conglomerate, affecting the overall dielectric properties of the material [105, 106, 110]. Additionally, it is well known that hydrogen bonding has a significant effect on capillary-driven processes [162, 189, 191, 192]. Also, hydrogen bonds are involved in proton transfer reactions and may be considered partially activated precursors of such reactions [105, 106, 110]. Similarly, sucrose molecules in aqueous solutions can remain immobile as protons are passing through the concentrated solutions, similarly to a Grotthuss chain mechanism [110]. Also, extensive secondary bonding can potentially increase the predicted molecular relaxation times for supramolecular solutions, especially when confined under electrical stresses [10, 11].

However, the electrospinnability of octa-*O*-acetyl sucrose challenges the argument for reciprocal hydrogen bonding electrospinnability. Moreover, such evidence suggests that electrospinnability might be driven by van der Waals forces and to a lesser extent by hydrogen bonding, as suggested by the properties and behaviour of octa-*O*-methyl sucrose. Nevertheless, no conclusive proof of either hydrogen bonding interactions (H-donors / H-acceptors) or permanent nor induced dipolar moments, can be categorically correlated to the electrospinnability of octa-*O*-acetyl sucrose. Nonetheless, the apparent hydrogen-accepting capacity and molecular polarity of the tested concentrated solutions were definitely an important requirement for the electrospinnability of tested materials.

Remarkably, glucose syrup, concentrated saccharide solutions, cyclodextrin mixtures and modified sucrose compounds all showed similar trends associated with their electrospinnability; Higher density, higher than average surface tension values at higher concentrations, lower conductivities at higher concentrations and higher pH values; all promoted electrospinnability of tested materials. Decisively, conductivity alone is not a determining factor to the electrospinnability of tested materials, since there is not a consistent linear relationship between conductivity and other physical-chemical variables in tested saccharide systems. Also, the overall effects of the viscoelastic properties of the materials undergoing a capillary thinning process were of significant

importance to the electrospinnability of tested materials. Conclusively, the relations between hydrogen donor-acceptor interactions, van der Waals forces, and other complex electrodynamic interactions caused by the high voltages that drive the electrospinning process in respect to the material's entanglement condition and associated visco-elasto-capillary properties, are highly complex.

Acknowledgements

The authors thank the Ministry of Business Innovation and Employment of New Zealand (MBIE) for financial support. Author (PGTL) is particularly grateful to the National Institute of Science and Technology of Mexico (CONACYT) for financial assistance. The technical assistance from the NZ Institute for Plant and Food Research Ltd., Mr Neil Buunk of Electrospinz Ltd., and from Revolution Fibres Ltd. is also gratefully acknowledged.

Compliance with Ethical Standards

This study was funded by the University of Canterbury and Plant and Food Research Ltd., through a joint PhD studentship received from the Ministry of Business Innovation and Employment of New Zealand (MBIE) granted through Revolution Fibres Ltd., and by a PhD scholarship from the National Institute of Science and Technology of Mexico (CONACYT) granted to Pablo Lepe. No private funding was received from any other Company or external organization. All authors declare that there is no conflict of interest related to the publication of this manuscript.

References:

1. Davis B., and Fairbanks A. Carbohydrate chemistry. Oxford Chemistry Primers, 2002;1:1-100.
2. Garg H., Cowman M. and Hales C. Carbohydrate chemistry, biology and medical applications. Oxford - Elsevier, 2008; 1:1-414.
3. Pérez, A. Thermodynamic properties of sugars in aqueous solutions: correlation and prediction using a modified UNIQUAC model. Fluid phase equilibria, 1996; 123:71-95.
4. Boddohi S. Engineering Nano assemblies of polysaccharide. Advanced materials, 2010; 22:2998–3016.
5. Jansson H.Dynamics of sugar solutions as studied by dielectric spectroscopy. Journal of non–crystalline solids, 2005; 351:2858-2863.
6. Fabri Deborah. Water t2 relaxation in sugar solutions. Carbohydrate research, 2005; 340:889-905.
7. Ziabicki A. Fundamentals of fibre formation, John Wiley and Sons, 1976, 1:1-504.
8. Eichhorn S., Hearle J., Jaffe M., and Kikutani T. Fundamentals and manufactured polymer fibres. Handbook of textile fibre structure. CRC, 2009; 1:1-528.
9. Barber R. The influence of Knudsen number on the hydrodynamic development length within parallel plate micro-channels. Advances in fluid mechanics, 2002; 4:207-216.
10. Myers D. Surfaces, Interfaces and Colloids; Principles and Applications. Wiley–VCH, 1999; 2:1-528.
11. Ninham W., and Lo Nostro P. Molecular forces and self-assembly; in colloid, nano sciences and biology. Cambridge University Press, 2010; 1:1-360.
12. Yarin A., Kommbhongse S., and Reneker H. Bending instability in electrospinning of nanofibres. Journal of Applied Physics, 2001; 89:3018-3026.
13. Greiner H. and Wendorff J. Self-Assembled nanomaterials 1; nanofibres. Advances in polymer science, 2008; 219:1-175.
14. Tirtaatmadja V. Drop formation and breakup of low viscosity elastic fluids: Effects of molecular weight and concentration. Physics of fluids, 2006; 18:1-17.
15. McKinley G. Dimensionless Groups for understanding free surface flows of complex fluids. Rheology Bulletin, 2005; 1:1-8.

16. McKinley G. Visco-Elasto-Capillary Thinning and Break up of complex fluids, MIT – report, 2005; 1:1-49.
17. Doyle P., Shaqfeh E., McKinley G., and Spiegelberg S. Relaxation of dilute polymer solutions following extensional flow. Journal of Non-Newtonian Fluid Mechanics, 1997; 76:79-110.
18. McKinley G. Iterated stretching and multiple beads-on-a-string phenomena in dilute solutions of highly extensible flexible polymers. Physics of fluids, 2005; 17:1-5.
19. McKinley G. Dimensionless Groups for understanding free surface flows of complex fluids. Rheology Bulletin, 2005; 1:1-8.
20. De Gennes P. Scaling concepts in polymer physics. Cornell University Press, 1979, Ithica; 1:1-321.
21. Chen Z., Mo X., He C., and Wang H. Intermolecular interactions in electrospun collagen-chitosan complex nanofibres. Carbohydrate Polymers, 2008; 72:410-418.
22. Schiffman J., and Schauer C. A review: Electrospinning of biopolymer nanofibres and their applications. Polymer Reviews, 2008; 48:317-352.
23. Desiraju G., and Steiner T. The weak hydrogen bond in structural chemistry and biology. Monographs on Crystallography, 2001; 9:1-526.
24. Manasco J. L., Tang C., and Khan S. A. Cyclodextrin fibres via polymer–free electrospinning. RSC Advances, 2012; 2:3778-3784.
25. Uyar T., and Celebioglu A. Electrospinning of Polymer–free Nanofibres from Cyclodextrin Inclusion Complexes. Langmuir, 2011; 27:6218-6226.
26. Uyar T., and Kayaci F. Solid Inclusion Complexes of Vanillin with Cyclodextrin: Their Formation, Characterisation, and High–Temperature Stability. Journal of agricultural and food chemistry, 2011; 59:11772-11778.
27. Uyar T., and Celebioglu A. Cyclodextrin nanofibre by electrospinning. Chem. Commun., 2010; 46:6903-6905.
28. Wang X., Pellerin C., and Bazuin C. Effect of small molecule hydrogen-bond crosslinker and solvent power on the electrospinnability of poly(4-vinyl pyridine). Polymer, 2015; 57:62-69.
29. Son W., Youk J., Lee T., and Park W. Effect of pH on the electrospinning of poly (vinyl alcohol). Materials Letters, 2005; 59:1571-1575.
30. McKee M., Elkins C., and Long T. Influence of self-complementary hydrogen bonding on solution rheology/electrospinning relationships. Polymer, 2004; 45:8705-8715.

31. Rossi B., Gomez, L., Fioretto D., Caponi S., and Rossi F. Hydrogen bonding dynamics of cyclodextrin–water solutions by depolarized light scattering. J. Raman Spectroscopy, 2011; 42:1479-1483.
32. Celebioglu A., and Uyar T. Electrospinning of nanofibres from non-polymeric systems: polymer-free nanofibres from cyclodextrin derivatives. Nanoscale, 2012; 4:621-631.
33. Lee K., Jeong L., Kang Y., Lee S., and Park W. Electrospinning of polysaccharide for regenerative medicine. Advanced Drug Delivery Reviews, 2010; 61:1020-1032.
34. Manandhar S., Vidhate S and D'Souza N. Water soluble levan polysaccharide biopolymer electrospun fibres. Carbohydrate Polymers, 2009; 78:794-798.
35. Madhurima J., and Sanjoy B. Vibrational spectrum of water confined in and around cyclodextrin. Chemical Physics Letters, 2011; 509:181-185.
36. Charalampopoulos V., and Papaioannou J. Dipole relaxation and proton transport in polycrystalline γ–cyclodextrin hydrate: A dielectric spectroscopy study. Solid State Ionics, 2011; 191:1–11.
37. Challa R., Ahuja A., Ali, J., and Khar R. Cyclodextrin in drug delivery: An updated review. AAPS Pharm Sci Tech., 2005; 6:329-357.
38. Celebioglu A., and Uyar T. Electrospinning of nanofibres from non-polymeric systems: Electrospun nanofibres from native cyclodextrin. Journal of Colloid and Interface Science, 2013; 404:1-7.
39. Stijnman A., Bodnar I. and Tromp R. Electrospinning of food-grade polysaccharide. Food Hydrocolloid, 2011; 25:1393-1398.
40. Boland E. Electrospinning of Biopolymers (Natural and Synthetic) for Tissue Engineering Scaffolds. Polymer Preprints, 2003; 44:92-93.
41. D. Hermida-Merinoa, Belalb M., Greenlanda B., Woodwarda P., Slarkc A., Davisa F., Mitchellb G., Hamleya I., and Hayesa W. Electrospun supramolecular polymer fibres. European Polymer Journal, 2012; 48:1249-1255.
42. Alvarez-S. J., Gasparrini M., Forbes-H. T., Mazzoni L., and Giampieri F. The composition and biological activity of honey: a focus on mānuka honey. Foods, 2014; 3:420-432.
43. Crespy D., Friedemann K., and Popa A-M. Colloid-Electrospinning: Fabrication of Multicompartment Nanofibers by the electrospinning of Organic or/and Inorganic Disperns and Emulsions. Macromolecular Rapid Communications, 2012; 1:978-1995.

44. Angeles M., Cheng H-L., Velankar S. Emulsion electrospining: Composite fibers from drop breakup during electrospinning. Polym. Adv. Technol,. 2008; 1:728-733.
45. Xu X., Zhuang X., Chen X., Wang X., Yang L., and Jin X. Preparation of Core-Sheath Composite Nanofibers by Emulsion Electrospinning. Macromol. Rapid Commun., 2006; 27:1637-1642.
46. Agarwal S., and Greiner A. On the way to clean and safe electrospinning-green electrospinning: emusion and suspension electrospinning. Polym. Adv. Technol. 2012; 22:372-378.
47. Bosman A., Sijbesma R., and Meijer E. Supramolecular polymers at work. Materials today, 2004; 1:34-39.
48. Greef T., and Meijer E. Supramolecular Polymers. Aust. J. Chem. 2010; 63:596-598.
49. Gittins, P., and Twyman, L. Dendrimers and Supramolcular Chemsitry. Supramolecular Chemistry, 2003; 15:5-23.
50. Del-Valle E. Cyclodextrin and their uses: a review. Process Biochemistry, 2004; 39:1033-1046.
51. Okimoto K., Uekama K., and Stella J. The interaction of charged and uncharged drugs with nuetral (HP-Beta-CD) and anionically charged (SBE6-Beta-CD) Beta-Cyclodextrin. Pharmaceutical Research, 1996; 13:256-264.
52. Parkar S., Jobsis C.,Herath T., Stoklosinski H., Klink J., Sansom C., Sims I., and Hedderley D. Metabolic and microbial responses to the complexation of mānuka honey with α-cyclodextrin after simulated gastrointestinal digestion and fermentation. Journal of functional foods, 2017; 31:266-273.
53. Manasco J., Tang C., and Khan S. Cyclodextrin fibres via polymer-free electrospinning. RSC Advances, 2012; 2:3778-3784.
54. Martin C. Stumpe and Helmut G. Aqueous Urea Solutions: Structure, Energetics, and Urea Aggregation. Journal of Physical Chemistry, 2007; 111:6220-6228.
55. Coleman A., and Nicolis I. Aggregation of Cyclodextrins: An explanation of the abnormal solubility of β-Cyclodextrin. Journal of Inclusion Phenomena and Molecular Recognition in Chemistry, 1992; 13:139-143.
56. Carr J., Buchanan L., Schmidt J., Zanni M., and Skinner J. Structure and Dynamics of Urea/Water Mixtures Investigated by Vibrational

Spectroscopy and Molecular Dynamics Simulation. Journal of Physical Chemistry B., 2013; 1147:13291-13300.
57. Nose A. and Hojo M. Hydrogen bonding of water-ethanol in alconolic beverages. Journal of Bioscience and Bio-engineering, 2006; 112:269-280.
58. Idrissi A., and Jedlovszky P. Hydration free energy difference of acetone, acetamide, and urea. J. Chem. Phys., 2008; 129:291-300.
59. Wang X., Pellerin C., and Bazuin C. Enhancing the electrospinnability of low molecular weight polymers using small effective cross-linkers. Macromolecules, 2016; 49:891-899.
60. Stijnman A., Bodnar I. and Tromp R. Electrospinning of food-grade polysaccharide. Food Hydrocolloid, 2011; 25:1393-1398.
61. Dong B., Arnoult O., Smith M., and Wnek G. Electrospinning of collagen nanofibre scaffolds from benign solvents. Macromolecular Rapid Communications, 2009; 30:539-542.
62. Hofman K., Tucker N., Stanger J., Staiger M., Marshall S., and Hall B. Effects of the molecular format of collagen on characteristics of electrospun fibres. Journal of Materials Science, 2012; 47:1148-1155.
63. Yao C., X.S. Li and T.Y. Song, Electrospinning and crossfinking of Zein nanofibre mats. Journal of Applied Polymer Science, 2007; 103:380-385.
64. Selling G., Woods K., Sessa D., and Biswas A. Electrospun zein fibres using glutaraldehyde as the crosslinking reagent: Effect of time and temperature. Macromolecular Chemistry and Physics, 2008; 209:1003-1011.
65. Selling G.W., Biswas A., Patel A., Walls D., Dunlap C., and Wei Y. Impact of solvent on electrospinning of zein and analysis of resulting fibres. Macromolecular Chemistry and Physics, 2007; 208:1002-1010.
66. Miyoshi T., K. Toyohara and H. Minematsu Preparation of ultrafine fibrous zein membranes via electrospinning. Polymer International, 2005; 54:1187-1190.
67. Jiang H., Zhao P., and Zhu K. Fabrication and characterisation of zein-based nanofibrous scaffolds by an electrospinning method. Macromolecular Bioscience, 2007; 7:517-525.
68. Woerdeman D., Ye P., Shenoy S., Parnas R., Wnek G., and Trofimova O. Electrospun fibres from wheat protein: Investigation of the interplay between molecular structure and the fluid dynamics of the electrospinning process. Biomacromolecules, 2005; 6:707-712.

69. Kowalczyk T., Nowicka A., Elbaum D., and Kowaleski T. Electrospinning of bovine serum albumin. Optimization and the use for production of biosensors. Biomacromolecules, 2008; 9:2087-2090.
70. Wnek G., Carr M., Simpson D., and Bowling G. Electrospinning of Nanofibre Fibrinogen Structures. Nano Letters, 2003; 3:213-216.
71. Dror Y.,Ziv T., Makarov V., Wolf H., Admon A., and Zussman E. Nanofibres made of globular proteins. Biomacromolecules, 2008; 9:2749-2754.
72. Huang Z., Zhang Y., Ramakrishna S., and Tim C. Electrospinning and mechanical characterisation of gelatin nanofibres. Polymer, 2004; 45:5361-5368.
73. Zhang Y., Ouyang H., Lim C., Ramakrishna S., and Huang Z. Electrospinning of gelatin fibres and gelatin/PCL composite fibrous scaffolds. Journal of Biomedical Materials Research, 2004: 1:156-165.
74. Mo X., Xu C., Kotaki M. and Ramakrishna, S. Electrospun PLA-PCL nanofibre: A biomimetic extracellular matrix for smooth muscle cell and endothelial cell proliferation. Biomaterials, 2004; 25:1883-1890.
75. Boland E. Electrospinning of Biopolymers (Natural and Synthetic) for Tissue Engineering Scaffolds. Polymer Preprints, 2003; 44:92-93.
76. Kidoaki S., Kwon I., and Matsuda T. Mesoscopic spatial designs of nano- and microfibre meshes for tissue-engineering matrix and scaffold based on newly devised multilayering and mixing electrospinning techniques. Biomaterials, 2005; 26:37-46.
77. Martino A., Sitinger M., and Risbud M. Chitosan: A versatile biopolymer for orthopaedic tissue-engineering. Biomaterials, 2005; 26:5983-5990.
78. Ohkawa K., Cha D., Kim H., Nishida A., and Yamamoto H. Electrospinning of chitosan. Macromolecular Rapid Communications, 2004; 25:1600-1605.
79. Duan B., Zhu, Y., Yuan X., Zhang Y., Li X., and Yao K. A nanofibrous composite membrane of PLGA-chitosan/PVA prepared by electrospinning. European Polymer Journal, 2006; 42:013-2022.
80. Ignatova M., N. Manolova and I. Rashkov. Novel antibacterial fibres of quaternized chitosan and poly (vinyl pyrrolidone) prepared by electrospinning. European Polymer Journal, 2007; 43:1112-1122.
81. Lin T., Fang J., Wang H., Cheng T., and Wang X. Using chitosan as a thickener for electrospinning dilute PVA solutions to improve fibre uniformity. Nanotechnology, 2006; 17:3718-3723.

82. Bhattarai N., Edmonson D., Veiseh O., Matsen F., and Zhang M. Electrospun chitosan-based nanofibres and their cellular compatibility. Biomaterials, 2005. 26: p. 6176-6184.
83. Frey M. Electrospinning cellulose and cellulose derivates. Polymer Reviews, 2008; 48:378-391.
84. Han S., Youk J., Min K., Kang Y., and Park W. Electrospinning of cellulose acetate nanofibres using a mixed solvent of acetic acid-water: Effects of solvent composition on the fibre diameter. Materials Letters, 2008; 62:759-762.
85. Chen L., Bromberg L., Hatton T., and Rutledge G. Electrospun cellulose acetate fibres containing chlorhexidine as a bactericide. Polymer, 2008; 49:1266-1275.
86. Liu H. and Hsieh Y. Ultrafine fibrous cellulose membranes from electrospinning of cellulose acetate. Journal of Polymer Science, 2002; 40:2119-2129.
87. Garg H., Cowman M. and Hales C. Carbohydrate chemistry, biology and medical applications. Oxford - Elsevier, 2008; 1:1-414.
88. Toskasa G., Hund F., Laourinne E., Cherif C., Smyrniotopolous V., and Roussis V. Nanofibres based on polysaccharide from the green seaweed Ulva Rigida. Carbohydrate Polymers, 2011; 84:1093-1102.
89. Li M., Mondrinos M., Gandhi M., Ko F., Weiss A., and Lelkes P. Electrospun protein fibres as materials for tissue engineering. Biomaterials, 2005; 26:5999-6008.
90. Schiffman J., and Schauer C. A review: Electrospinning of biopolymer nanofibres and their applications. Polymer Reviews, 2008; 48:317-352.
91. Duling R., Dupaix R., Katsube N., and Lannutti J. Mechanical characterisation of electrospun polycaprolactone (PCL): A potential scaffold for tissue engineering. Journal of Biomechanical Engineering, 2008; 130:1-9.
92. Okimoto K., Uekama K., and Stella J. The interaction of charged and uncharged drugs with nuetral (HP-Beta-CD) and anionically charged (SBE6-Beta-CD) Beta-Cyclodextrin. Pharmaceutical Research, 1996; 13:256-264.
93. Yarin A. Coaxil electrospining and emulsion electrospinning of core-shell fibers. Polym. Adv. Technol., 2011; 22:310-317.
94. Ray-S. S., Pelot D., Zhou P., Rahman A., Wu X., and Yarin A. Encapsulation f self-healing materilas by coelectrospining, emulsion,

electrospinning, solution blowing and intercalation. J. Mater. Chem., 2012; 22:9138-9146.
95. Yan S., Xiaoqiang L., Shuiping L., Xiumei Mo., and Ramakrishna S. Controlled release of dual drugs form emulsion electrospin nanofibrous mats. Collids and Surfaces B: Biointerfaces, 2009; 73:376-381.
96. Xu X., Yang L., Xu X., Wang X.,Chen X., Laing, Q., Zeng J., and Jing, X. Ultrafine medicated fibers electrospun from X/O emulsions. Journal of Controlled Release, 2005; 108:33-42.
97. Liao Y., Zhan L., Gao Y., Zhu Z-T., and Fond H. Preparation, characteriseation, and encapsulation/release stufies of a compoiste nanofiber mat electrospun from an emulcion containing poly(lactic-co-glycolic acid). Polymer, 2008; 48:5294-5299.
98. Friedemann K., Tomas C., Kappl M., Landfester K., and Crespy D. Facil and Large-Scale Fabrication of Anisometric Particles from Fibers Synthesized by Colloid-Electrospinning. Small, 2012; 1:144-153.
99. Stoiljkovic A., Venkatesh R., Klimov E., Raman V., Wendorff J., and Greiner A. Poly(styrene-co-n-butyl acrylate) Nanofibers with Excellent Stability against Water by Electrospinning from Aqueous Colloidal Dispersions. Macromolecules, 2009; 42:6147-6151.
100. Garg H., Cowman M. and Hales C. Carbohydrate chemistry, biology and medical applications. Oxford - Elsevier, 2008; 1:1-414.
101. Lepe P., Tucker N., Simmons L., Watson A., Fairbanks A., and Staiger M. Submicron sized saccharide fibres via electrospinning. De Gruyter Open – Electrospinning, 2016; 1:p.1-9.
102. Poland D., and Scheraga H. Energy Parameters in Polypeptides I: Charge distributions and the hydrogen bond. Biochemistry, 1967; 6:3791-3800.
103. Yan J., Momany F., Hoffmann H., and Scheraga H. Energy Parameters in Polypeptides II: Semi empirical Molecular Orbital Calculations for model peptides. Physical chemistry, 1970; 74:420-433.
104. Yan J., Momany F., Hoffmann H., and Scheraga H. Energy Parameters in Polypeptides III: Semi empirical Molecular Orbital Calculations for Hydrogen–Bonded Model Peptides. Physical Chemistry, 1970; 74:2424-2438.
105. Akira H. Supramolecular Polymer Chemistry. Wiley – VCH, 2011; 1:1-361.
106. Onsager L. Electrostatic interaction of molecules. Journal of Physical Chemistry, 1939; 43:189-196.

107. Wan Y., He J., and Yu J. Allometric scaling and instability in electrospinning. International journal of nonlinear sciences and numerical simulations, 2004; 5:243-252.
108. Van Honschoten J., Tas N., and Brunets N. Capillarity at the nanoscale. Chemical society reviews, 2009; 39:1096-1114.
109. Wautelet M., Scaling laws in the macro, micro and nanoworlds. Institute of Physics Publishing, 2001; 22:601-611.
110. Israelachvili J. Intermolecular and Surface Forces. Elsevier – Academic Press, 2011; 3:1-674.
111. Woerdeman D., Breger Di and Shenoy, S. Role of Chain Entanglements in the Electrospinning of Wheat Protein-Poly(Vinyl Alcohol) Blends. The Journal of Adhesion, 2007; 83:785-798.
112. Rubistein M., and Semenov A. Dynamics of Entangled solutions for associating polymers. Macromolecules, 2001; 34:1058-1068.
113. Monica S., Oliveira R., and McKinley G. Iterated stretching, extensional rheology and formation of beads-on-a-string structures in polymer solutions. J. Non-Newtonian Fluid Mech., 2006; 1:137-148.
114. Hiemenz P. Polymer chemistry: the basic concepts. CRC Press, 1984; 1:1-738.
115. Fujita H. Polymer solutions. Studies on polymer science. Elsevier – Netherlands, 1990; 9:1-370.
116. Terakota I. Polymer solutions: An introduction to physical properties. John Wiley & Sons, 2002; 1:1-349.
117. Freire J. Relaxation of flexible chains in dilute and non–dilute systems. Dynamic Monte Carlo results for linear and star chains. Macromolecules, theory simulations, 1999; 8:321-327.
118. Genotelle J., and Mathlouthi M. Role of water in sucrose crystallization. Carbohydrate polymers, 1998; 37:335-342.
119. Quintas M., Brandao T., Silva C., and Cunha R. Rheology of supersaturated sucrose solutions. Journal of Food Engineering, 2006; 77:844-852.
120. Crest J., and McKinley G. Formation of microfibres and nanofibres by capillary-driven thinning of drying viscoelastic filaments. MIT report, 2009; 1:1-43.
121. Yu J., and Rutledge G. The role of elasticity in the formation of electrospun fibres. Polymer, 2006. 47:4789-4797.

122. Celebioglu A., and Uyar T. Electrospinning of nanofibres from non-polymeric systems: Electrospun nanofibres from native cyclodextrin. Journal of Colloid and Interface Science, 2013; 404:1-7.
123. Arunan E. Categorizing hydrogen bonding and other intermolecular interactions. Pure Applied Chemistry–IUPAC recommendation, 2011; 1:1-5.
124. Luzar A. Resolving the hydrogen bond dynamics conundrum. Journal of chemical physics, 2000; 113:10663-10675.
125. Boltachev G., and Baidakov V. Extended version o the Van der Waals capillarity theory. Journal of Chemical Physics, 2004; 121:8594-8601.
126. Kloosterman M., Weijnen J., De Vries N., Mentech J., Caron I., Descotes G. Schoemaker H., and Meijer E. Octa-O-acetyl sucrose: Regioselective deacetylations by lipolytic enzymes. Journal of Carbohydrate Chemistry, 1989; 8:1-8.
127. Fernandez-L. G., Palomo J., Cocca J., Mateo, C., Moro P., Terreni M., Fernandez-L. R., and Guisan J. Regio-selective deprotection of peracetylated sugars via lipase hydrolysis. Tetrahedron, 2003; 59:5705-5711.
128. Navzer S., Redford F., and Morton L. Use of sucrose-based addtivies as non-crosslinking agents to produce polymers having enhanced thermal stability. Patent no.5470931USPTO, 28 of February 1994; USA.
129. Thompson C., Chase G., Yarin A., and Reneker D. Effects of parameters on nanofibre diameter determined from electrospinning model. Polymer, 2007; 48:6913-6922.
130. Hohman M. Electrospinning and electrically forced jets II. Applications. Physics of fluids, 2001; 13:2221-2236.
131. Fridrikh S., Brenner M., and Rutledge G. Controlling the fibre diameter during electrospinning. Physical review letters, 2003; 90:144502-144506.
132. Subbiah T., Tock R., Parameswaran S., and Ramkumar S. Electrospinning of nanofibres. Applied polymer science, 2004; 96:557-569.
133. Reneker D., Yarin A., Fong H., and Koombhongse S. Bending instability of electrically charged liquid jets of polymer solutions in electrospinning. Journal of Applied Physics, 2000; 87: 4531-4547.
134. Qin X., Effect of Different Salts on Electrospinning of Polyacrylonitrile (PAN) Polymer Solution. Journal of Applied Polymer Science, 2007; 103:3865-3870.

135. Pavlov G., Korneeva E., Smolina N., and Schubert U. Hydrodynamic properties of cyclodextrin molecules in dilute solutions. European Biophysics Journal, 2010; 39:371-379.
136. Sabadini E., Cosgrovea T. and Egídio F. do C. Solubility of cyclomaltooligosaccharides (cyclodextrins) in H2O and D2O: a comparative study, Carbohydrate Research, 2006; 341:270-274.
137. Sinnott M. L. Carbohydrate chemistry and biochemistry. Royal Society of Chemistry, 2007; 1:1-748.
138. China air 2015: Air pollution prevention and control progress in Chinese cities. Clean Air Asia - Beijing, 2016; 1:1-80.
139. KPMG. China's connected consumers. KPMG, Hong Kong, 2015;1:1-74.
140. Quan M., and Junjie Z. Air pollution and defense expenditures: evidence from particulate-filtering facemasks. UCSD, 2014;1:1-47.
141. Cao J., Xu H., Xu Q., Chen B., and Kan H. Fine particulate matter constituents and cardiopulmonary mortality in a heavily polluted Chinese city. Environmental Health Perspectives, 2012; 120:373-378.
142. He Q., Guo W., Zhang G., Yan Y., and Chen L. Characteristics and seasonal variations of carbonaceous species in PM2.5 in Taiyaun, China. Atmosphere, 2015; 6:1-13.
143. Fang T., and Lin C. Minimum wages and employment in China. Journal of Labor Policy, 2015; 4:1-30.
144. Loungani Y-H., and Wang G. Minimum wages and firm employment: evidence from China. International Monetary Fund (IMF), 2014;1:1-47.
145. Hung C-H., and Leung W. Filtration of nano-aerosol using nanofiber filter under low peclet number and transitional flow regimen. Separation and Purification Technology, 2011; 79:34-42.
146. Sudanrrajan S., Tan K., Lim S., and Ramakrishna S. Electrospun nanofibers for air filtration applications. Procedia Engineering, 2014; 75:159-163.
147. Qin W-H., and Wang S-Y. Filtration properties of electrospinning nanofibers. Journal of Applied Polyer Science, 2006; 102:1285-1290.
148. Ellision C., Melt blown nanofibers: Fiber diameter distributions and onset of fiber breakup. Polymer, 2007; 48:3306-3316.
149. Wang S-X., Yap C., He J., Chen C., and Wong S. Electrospinning: a facile technique for fabricating functional nanofibers for environmental applications. Nanotechnol Rev., 2016; 5:51-73.

150. Bhardwaj Nandana. Electrospinning: A fascinating fibre fabrication technique. Biotechnology/Advances, 2010; 28:325-347.
151. Wendorff J. Functional Self-Assembled Nanofibres by Electrospinning. Advances on Polymer Science, 2008; 1:107-171.
152. Hofman K., Ion exchange HPLC of a marine collagen. Journal of Liquid Chromatography and related technologies, 2009; 17:2512-2529.
153. Hofman K., Hall B., Cleaver H., and Marshall S. High-throughput quantification of hydroxyproline for determination of collagen. Analytical Biochemistry, 2011; 417:289-291.
154. Hofman K., and Newberry M. Thermal transition properties of Hoki (Macruronus novaezelandiae) and Ling (Genypterus blacodes) skin collagens: Implications for processing. Marine drugs, 2011; 9:1176-1186.
155. Shenoy S., Bates W., Frish H., and Wnek G. Role of chain entanglements on fibre formation during electrospinning of polymer solutions: good solvent, non-specific polymer-polymer interaction limit. Polymer, 2005; 46:3372-3384.

Table of Contents